J. Fluid Mech. (1985), *vol.* 157, *pp.* 95–134
Printed in Great Britain

The stability and energetics of corotating uniform vortices

By DAVID G. DRITSCHEL
Geophysical Fluid Dynamics Program, Princeton University, New Jersey 08540

(Received 12 June 1984 and in revised form 1 February 1985)

Equilibrium shapes of two-dimensional rotating configurations of uniform vortices are numerically calculated for two to eight corotating vortices. Additionally, a perturbation series is developed which approximately describes the vortex shapes. The equilibrium configurations are subjected to a linear stability analysis. This analysis both confirms existing results regarding point vortices and shows that finite vortices may destabilize via a new form of instability derived from boundary deformations. Finally, we examine the energetics of the equilibrium configurations. We introduce a new energy quantity called 'excess energy', which is particularly useful in understanding the constraints on the evolution of unstable near-equilibrium configurations. This theory offers a first glance at nonlinear stability. As an example, the theory explains some features of the merger of two vortices.

1. Introduction

A little more than a century ago, Thomson (1883) investigated the linear stability of corotating point vortices of equal strength. The vortices were equally spaced along the circumference of a circle. By perturbing the relative locations of the vortices, he found that six or fewer vortices are stable. The current study extends that of Thomson by examining the effect of finite vortex size. By a vortex, we mean a finite region of rotational fluid bounded by irrotational fluid in two-dimensional inviscid incompressible unbounded flow. We assume that an equilibrium state of the flow may consist of several identical regions of *uniform* vorticity whose boundaries are stationary when viewed from an appropriately rotating reference frame. By perturbing the boundaries of these finite-area vortices, we can determine their linear stability. In the limit of small vortices, the results reduce to those of Thomson.

We are generalizing Thomson's problem because finite vortices are thought to provide a more realistic model of fluid flow than do point vortices. The assumption of constant-vorticity vortices results in an important and useful simplification of the solution of the Euler equations – the velocity field at any point in space depends only upon the locations of the vortex boundaries (or contours) and the jumps of vorticity across them. This velocity field then advects the contours to a new arrangement. Thus the problem effectively becomes one-dimensional. This simplification was originally pointed out by Deem & Zabusky (1978*a*, *b*), who called it 'contour dynamics'. They calculated the shapes of certain translating or rotating vortex states ('*V*-states'). Subsequently, numerous other researchers have taken an interest in the field. Steady solutions have been found by Pierrehumbert (1980) for two opposite-signed symmetrical vortices, Saffman & Szeto (1980) for two like vortices (duplicated in the present work), Pierrehumbert & Widnall (1981) for an infinite row of identical vortices, and Saffman & Schatzman (1982) for the von Kármán vortex street (two opposite-signed

infinite rows of identical vortices). Saffman & Schatzman were also the first to examine the stability of constant-vorticity vortices. In the current study we will carefully detail how the stability problem is set up and then solve for the stability of equilibrium configurations of corotating vortices.

The present investigation may have some relevance to the dynamics of clusters of organized vortices in a free shear layer, where vortex fission and merger are commonplace events (see Christiansen & Zabusky 1973). Nonlinear calculations by Overman & Zabusky (1982) suggest that fission and merger result from complex nonlinear behaviour. Our linear calculations afford no hope of understanding these phenomena, but we will discuss a new energy theory which highly constrains nonlinear evolution. Dritschel (1985) examines the nonlinear evolution and stability of vortex configurations and shows that the current study's energy theory is very useful in understanding nonlinear behaviour.

We will consider equilibrium configurations of two to eight vortices. Section 2 covers the dynamics of piecewise-constant vorticity distributions ('contour dynamics') and then describes a numerical algorithm used to compute equilibrium vortex boundary shapes. In §3 we derive an approximate expression for the boundary shapes which is used to confirm the numerical results. Section 4 compares the approximate and exact solutions, and some peculiar properties of the exact solutions are indicated. We move to discuss linear stability – setting up the problem, simplifying it, and solving it – in §§5–7. In §8 we begin a discussion of energetics, where we announce a new and useful energy quantity. Section 9 points out the conserved global quantities in a two-dimensional fluid, while §10 illustrates how these quantities constrain the *non*linear evolution of vortices. There we also postulate the fate of various relevant unstable vortex configurations. We try to connect the linear stability results and the energy theory in §11, and then conclude in §12.

2. The vortex boundary shapes

2.1. *Mathematical review of vortex motion*

In this subsection we review the equations governing the evolution of vorticity distributions in two dimensions and the special form attained by these equations when the vorticity is piecewise-constant. An equivalent derivation has been given by Zabusky, Hughes & Roberts (1979). For an unbounded fluid with a vorticity distribution $\omega(x,y)$ the streamfunction $\psi(x,y)$ is given by

$$\psi(x,y) = (2\pi)^{-1} \iint \mathrm{d}x'\,\mathrm{d}y'\,\omega(x',y')\log r, \tag{2.1}$$

where $r^2 = (x-x')^2+(y-y')^2$; this is obtained by solving $\nabla^2\psi = \omega$ in terms of the Green function of the problem. The velocity field is

$$\boldsymbol{u}(x,y) = (u,v) = (-\psi_y, \psi_x) = (2\pi)^{-1} \iint \mathrm{d}x'\,\mathrm{d}y'\,\omega(x',y')\,\frac{(-(y'-y),(x'-x))}{(x'-x)^2+(y'-y)^2}. \tag{2.2}$$

Now suppose $\omega(x,y)$ is constant within regions R_k, which divide all of space: $\omega(x,y) = \omega_k$ if $(x,y)\in R_k$. Then we have

$$\psi(x,y) = (2\pi)^{-1} \sum_k \omega_k \iint_{R_k} \mathrm{d}x'\,\mathrm{d}y'\,\log r, \tag{2.3}$$

$$\boldsymbol{u}(x,y) = (2\pi)^{-1} \sum_k \omega_k \iint_{R_k} \mathrm{d}x'\,\mathrm{d}y'\,\frac{(-(y'-y),(x'-x))}{r^2}. \tag{2.4}$$

We next use Stokes' Theorem,

$$\iint_R (Q_{x'} - P_{y'})\,\mathrm{d}x'\,\mathrm{d}y' = \int_C (P\,\mathrm{d}x' + Q\,\mathrm{d}y'), \tag{2.5}$$

to convert the expressions for ψ and $\boldsymbol{u}$ into line integrals. C in Stokes' Theorem represents the entire boundary around the region R. Using $Q = \frac{1}{2}(x'-x)\log r$ and $P = -\frac{1}{2}(y'-y)\log r$ for ψ, we find that

$$\psi(x,y) = -(4\pi)^{-1}\Gamma + (4\pi)^{-1}\sum_k \omega_k \int_{C_k} \log r_k[(X_k - x)\,\mathrm{d}Y_k - (Y_k - y)\,\mathrm{d}X_k], \tag{2.6}$$

while, with $Q = 0$, $P = \log r$ for u and $Q = \log r$, $P = 0$ for v, we obtain

$$\boldsymbol{u}(x,y) = -(2\pi)^{-1}\sum_k \omega_k \int_{C_k} \log r_k\,\mathrm{d}\boldsymbol{X}_k, \tag{2.7}$$

where $r_k^2 = (X_k - x)^2 + (Y_k - y)^2$, $\boldsymbol{X}_k = (X_k, Y_k)$ is a point on C_k, the boundary of the region R_k, and Γ is the total circulation of the fluid:

$$\Gamma = \sum_k \omega_k A_k = \tfrac{1}{2}\sum_k \omega_k \int_{C_k} (X_k\,\mathrm{d}Y_k - Y_k\,\mathrm{d}X_k), \tag{2.8}$$

(A_k is the area of the region R_k). Both ψ and $\boldsymbol{u}$ involve an expression of the form

$$\sum_k \omega_k \int_{C_k} (\text{quantity independent of } \omega_k), \tag{2.9a}$$

and so this can be rewritten as

$$\sum_k \tilde{\omega}_k \int_{\tilde{C}_k} (\text{quantity independent of } \omega_k), \tag{2.9b}$$

where $\tilde{C}_k$ is the exterior boundary to R_k (there may be interior boundaries that are the exterior boundaries of other regions) and $\tilde{\omega}_k$ is the jump in the vorticity across $\tilde{C}_k$ (inside vorticity (ω_k) − outside vorticity). Now the dynamical evolution of the vortex boundaries $\tilde{C}_j$ is given by

$$\frac{\mathrm{d}\boldsymbol{X}_j}{\mathrm{d}t} = \boldsymbol{u}(\boldsymbol{X}_j) = -(4\pi)^{-1}\sum_k \tilde{\omega}_k \int_{\tilde{C}_k} \log[(X_k' - X_j)^2 + (Y_k' - Y_j)^2]\,\mathrm{d}\boldsymbol{X}_k'. \tag{2.10}$$

2.2. *Steadily corotating vortices*

The condition for a steadily rotating vortex configuration (relative to the origin at $(x,y) = (0,0)$) is that the fluid velocity measured in a frame rotating at a rate Ω is tangent to the vortices' boundaries. Ω is the constant rotation rate of the system. This is equivalent to saying that the rotating-frame stream function must be constant on the vortices' boundaries:

$$\psi(\boldsymbol{X}_j) - \tfrac{1}{2}\Omega(X_j^2 + Y_j^2) = C, \text{ a constant for each vortex}, \quad j = 1, \ldots, N.$$

This study is concerned with equilibrium configurations of the type shown in figure 1. Each vortex is identical with the others. The vorticity in each vortex is ω_0, a_0^* is the closest distance from the origin along a ray passing through the centre of the vortex, and a_1^* is the furthest distance. The geometry of the system is completely given by the function $g(\theta)$, which depends parametrically only on $a_0 = a_0^*/a_1^*$ and N, the number of vortices (we have restricted ourselves to symmetric solutions that have $g(\theta) = g(-\theta)$). The system is non-dimensionalized such that $\omega_0 = 1$ and $a_1^* = 1$. Then

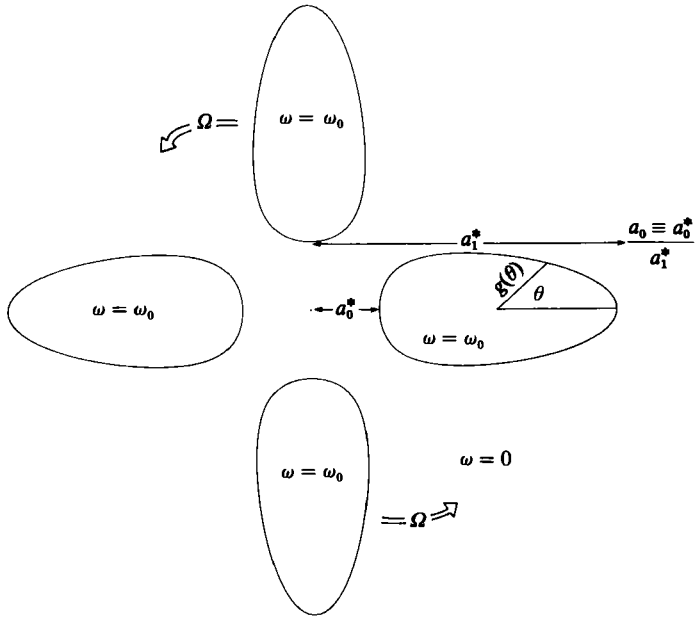

FIGURE 1. The geometry of $N = 4$ corotating constant-vorticity vortices.

the equilibrium solution is $[g(\theta; a_0, N), \Omega(a_0, N)]$ – for a given number of vortices, $a_0 < 1$ describes the family of solutions.

We had to resort to numerical means to find the equilibrium boundary shapes. We followed the numerical procedure outlined by Pierrehumbert (1980) with minor modifications specific to corotating configurations; thus only a brief discussion will be presented. Since all of the vortices are assumed to be identical and symmetric ($g(\theta) = g(-\theta)$), it is necessary only to calculate the boundary shape of the upper half of the vortex lying on the positive x-axis. Along this boundary

$$(x, y) = (r_0 + g(\theta)\cos\theta,\ g(\theta)\sin\theta),$$

where $r_0 = \frac{1}{2}(1-a_0)$ (see figure 1). The constancy of the stream function in the rotating frame then gives for every θ

$$C = \psi(g(\theta), \theta) - \tfrac{1}{2}\Omega(r_0^2 + g^2(\theta) + 2r_0 g(\theta)\cos\theta), \tag{2.11}$$

where ψ is calculated from (2.6). The two boundary conditions

$$g(0) = g(\pi) = R = \tfrac{1}{2}(1-a_0)$$

determine Ω and C as follows:

$$\Omega = 2\,\frac{\psi(0)-\psi(\pi)}{1-a_0^2}, \quad C = \psi(0) - \tfrac{1}{2}\Omega. \tag{2.12}$$

Thus (2.11) is a nonlinear integral equation to determine $g(\theta)$. Pierrehumbert (1980) introduced an iterative relaxation scheme whereby an equation like (2.11) was linearized about a good guess for the boundary shape in order to determine the correction to this shape. After a few iterations, we accepted the approximate solution as the exact solution when the relative error between two successive iterated

solutions fell below 10^{-4}. The scheme failed to converge only when the velocity tangent to the vortex boundary (in the rotating frame) approached zero somewhere along the boundary. Such a situation is known to give rise to 'corners' (see Wu, Overman & Zabusky 1982). Finally, in order to perform the contour integrals in the expressions for ψ and $\boldsymbol{u}$, we discretized the boundaries of the vortices. We chopped each boundary into 144 equal angles, interpolated the boundary between every two nodes by local cubics, and used 4-point Gaussian quadrature to integrate between every pair of nodes. The sum of all these integrals comprised the contour integral. The error introduced by the discretization was found to be well below 10^{-4} (we confirmed this by doubling the number of nodes on each vortex boundary). More specific details regarding the discretization can be found in Dritschel (1985).

3. The vortex boundary shapes: perturbation expansion

A perturbation expansion to fourth order in the small parameter

$$\delta \equiv R/r_0 = (1-a_0)/(1+a_0)$$

was carried out as an independent confirmation of the numerical results. Specifically, the boundary shape and the rotation rate were expanded in powers of δ:

$$\left.\begin{aligned} g(\alpha) &= R(1+\delta g_1(\alpha)+\delta^2 g_2(\alpha)+\delta^3 g_3(\alpha)+\ldots), \\ \Omega &= \Omega_0(1+\delta\Omega_1+\delta^2\Omega_2+\delta^3\Omega_3+\ldots), \end{aligned}\right\} \tag{3.1}$$

where Ω_0 is the rotation rate of small circular pointlike vortices:

$$\Omega_0 = \tfrac{1}{4}(N-1)\,\delta^2 \tag{3.2}$$

(Thomson 1883, p. 97).

In §2 we used the fact that the boundary must be a streamline in a frame rotating at angular velocity Ω. This is equivalent to saying that the local velocity be exactly tangent to the boundary (for then no fluid would cross it). The mathematical expression for this is

$$\frac{\mathrm{d}y}{\mathrm{d}x} = \frac{\tilde{v}}{\tilde{u}}, \tag{3.3}$$

where $y = g(\alpha)\sin\alpha$, $x = r_0+g(\alpha)\cos\alpha$, and $(\tilde{u},\tilde{v}) = (u,v)+\Omega(y,-x)$ is the velocity in the rotating frame. This is the same as

$$\frac{1}{g}\frac{\mathrm{d}g}{\mathrm{d}\alpha} = \frac{\tilde{u}_r}{\tilde{u}_\theta}, \tag{3.4}$$

where $\tilde{u}_r$ and $\tilde{u}_\theta$ are the radial and tangential velocities in the rotating frame relative to the point $(r_0,0)$:

$$\left.\begin{aligned} \tilde{u}_r &= \tilde{u}\cos\alpha+\tilde{v}\sin\alpha, \\ \tilde{u}_\theta &= \tilde{v}\cos\alpha-\tilde{u}\sin\alpha. \end{aligned}\right\} \tag{3.5}$$

To calculate g_1, g_2, g_3 and so on, the expansions in (3.1) are substituted into (3.4), and the velocity field is calculated using (2.7). Like powers of δ yield integral equations for $g_m(\alpha)$ which also depend upon $g_1(\alpha),\ldots,g_{m-1}(\alpha)$. The functional form of each g_m was inferred from the numerical calculations described in §2. The integral equation for each g_m then reduced to a simple linear algebraic equation to determine the coefficient(s) of g_m's functional form. It was straightforward to carry out the integrals implied by (2.7), but the algebra is lengthy and not very illuminating. We

just mention that several important sums had to be evaluated which have the following values: letting $c_k = \cos(2\pi k/N)$,

$$\left.\begin{aligned} \sigma &= \sum_{k=1}^{N-1} \frac{c_k}{1-c_k} = \tfrac{1}{6}(N-1)(N-5), \\ \gamma &= \sum_{k=1}^{N-1} \frac{c_k}{(1-c_k)^2} = \tfrac{1}{180}(N^2-1)(N^2-19). \end{aligned}\right\} \tag{3.6}$$

The first was determined by Thomson (1883), while the second was found by the author and is important for g_4. Then, to fourth order in δ, we determined that

$$\left.\begin{aligned} g &= R(1+\delta^2\sigma\sin^2\alpha+\delta^3\tau\sin^2\alpha\cos\alpha+\delta^4(\mu+\nu\cos^2\alpha)\sin^2\alpha+\ldots), \\ \Omega &= \Omega_0(1+\delta^2\sigma+O(\delta^4)), \end{aligned}\right\} \tag{3.7}$$

where $\tau = -\frac{1}{4}(N-1)(N-3)$, $\mu = \sigma(\frac{3}{2}\sigma+N-1)$, and $\nu = \frac{2}{3}(3\sigma+N-1-\frac{9}{4}\sigma^2-\gamma)$. We could not determine Ω_4, because this depends upon g_5. In any case, these expansions were thoroughly confirmed by comparing them with the numerically computed solutions for $N = 2$–7. Section 4 shows a few of these comparisons.

4. Properties of the equilibrium solutions

We next describe the numerical solutions for 2–7 vortices, compare these solutions with the perturbation series developed in §3, and show how an expression based on the dynamics of point vortices very closely agrees with the results for finite-area vortices.

4.1. *Geometric properties of the equilibrium solutions*

Figures 2(*a–f*) depict the families of solutions for 2–7 vortices. Each boundary corresponds to a different value of a_0 starting from $a_0 = 0.95$ and decrementing by $\Delta a_0 = 0.05$ until solutions with smaller a_0 could no longer be found. The solution with the smallest value of a_0 that we were able to compute is included among each family of solutions. Two vortices become pear-shaped and flattened as a_0 decreases. The $O(\delta^2)$ term of (3.7) accounts for the flattening effect ($\sigma = -\frac{1}{2}$), while the $O(\delta^3)$ term corresponds to the pear shape ($\tau = \frac{1}{4}$). The $O(\delta^4)$ term causes additional flattening, but this effect is only 5 % at $a_0 = 0.1$. Three vortices remain surprisingly elliptical for all a_0. This is because $\tau = 0$ and $\sigma = -\frac{2}{3}$. The fourth-order term causes additional flattening. Four vortices are also flattened ($\sigma = -\frac{1}{2}$), and again have a pear shape ($\tau = -\frac{3}{4}$), but, since τ has changed signs from 2–4 vortices, the pear shape is oppositely orientated. ν is now positive (it is positive only for $N = 4$, 5 and 6), which implies additional thickening around $\theta = \frac{1}{4}\pi$, $\frac{3}{4}\pi$, $\frac{5}{4}\pi$, and $\frac{7}{4}\pi$ on each vortex, but μ being negative (only for $N = 2$, 3 and 4) implies additional thinning around $\theta = \frac{1}{2}\pi$ and $\frac{3}{2}\pi$. For five vortices $\sigma = 0$ accounts for the persistent nearly circular boundary shapes. τ is negative for $N \geqslant 4$, so that the pear shape of four vortices typifies that for $N > 4$. The fourth-order effect is small, but thickens the vortices near $\theta = \frac{1}{4}\pi$, etc. For six vortices σ becomes positive for the first time, so that the elliptical distortion is directed *tangent* to the circle that passes through the vortex centres. This effect becomes stronger as the number of vortices increases, and may be due to the fact that the configuration of vortices begins to locally resemble a straight street of vortices – the distortions seen here are very much like those found by Pierrehumbert & Widnall (1981). The third-order term (τ) is due to the curved geometry, however,

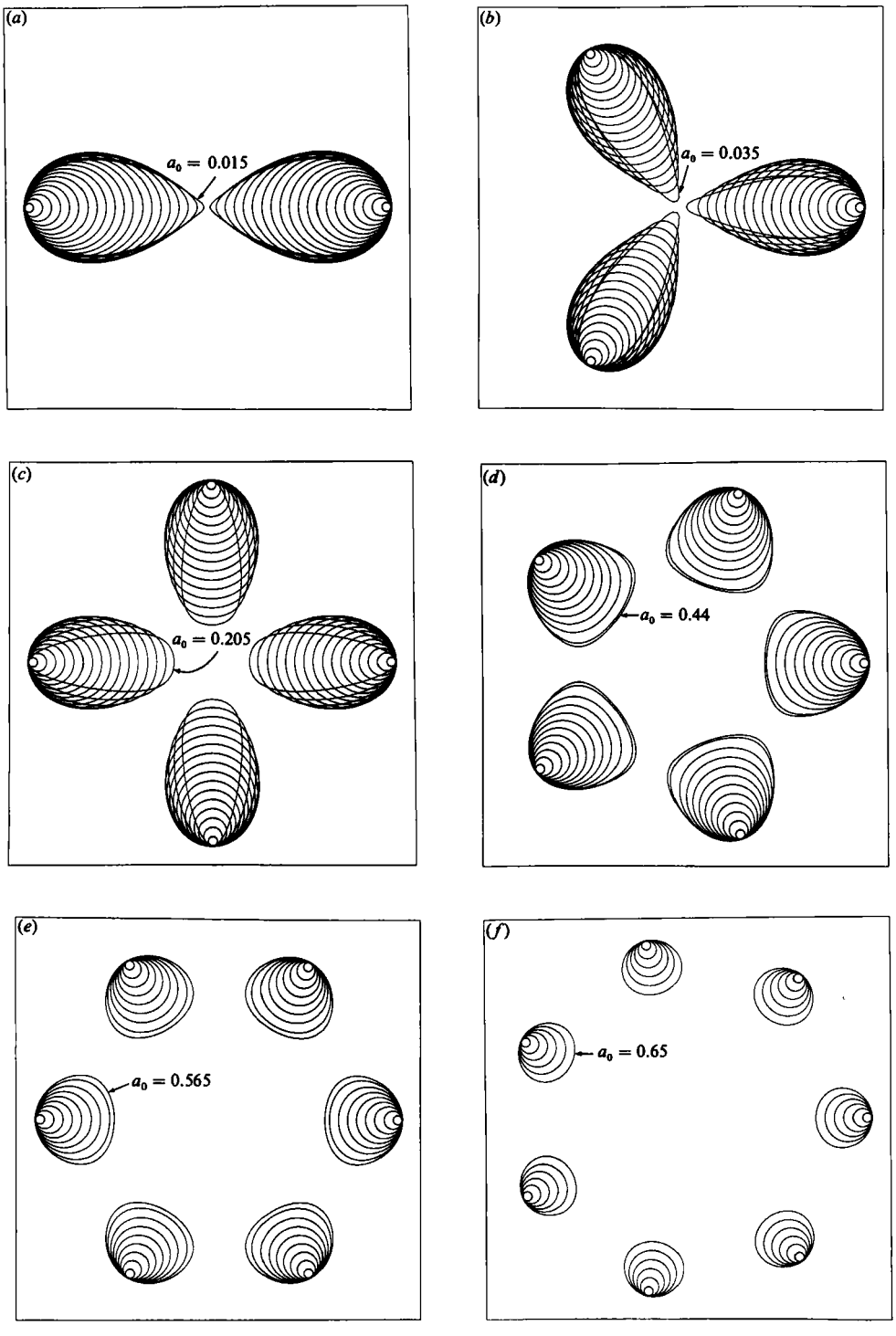

FIGURE 2. The superposition of the equilibrium solutions for various values of a_0, starting at $a_0 = 0.95$ and decrementing by $\Delta a_0 = 0.05$. The solution with the smallest a_0 that we were able to obtain is also indicated.

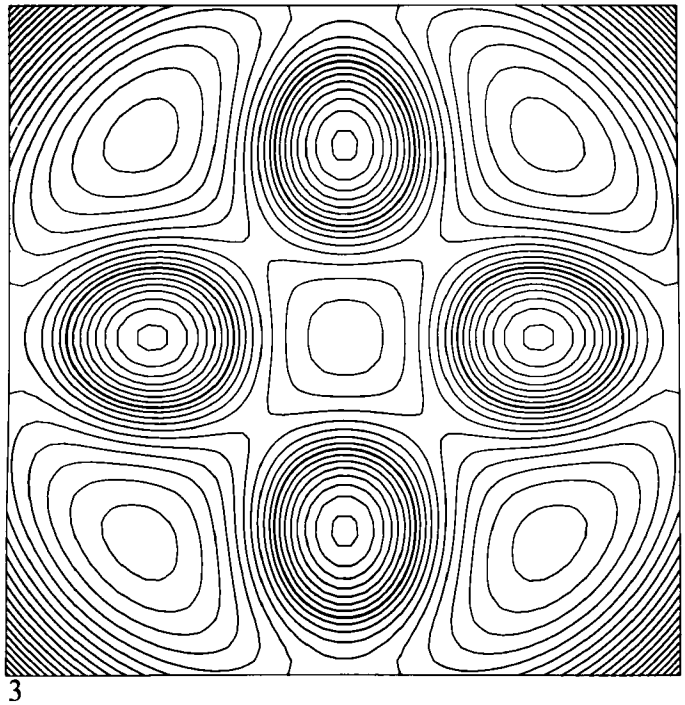

FIGURE 3. The rotating-frame stream-function field for 4 vortices with $a_0 = 0.4$, showing various distinct circulation regions. The bold contours denote the vortex boundaries.

and continues to distort each vortex into a pear shape. Since μ and ν are positive the elliptical shape is stretched (μ) but thickened at the ends (ν). For seven or more vortices ν becomes negative again ($\sigma > 0, \tau < 0, \mu > 0$), so that the elliptical shape is tapered at its ends. This tapering also occurs in the vortex-street solutions of Pierrehumbert & Widnall, who furthermore found that their family of distinct vortex solutions passes continuously into a family of wavy vortex-*sheet* solutions. By analogy, we expect that the families of corotating vortices pass continuously into families of wavy annular vortex solutions (curved vortex sheets) for large enough N. We suspect that four or more vortices may touch at points between themselves but not at the origin (Overman & Zabusky (personal communication 1984) have shown that two and three vortices touch at the origin when $a_0 = 0$).

4.2. *Confined fluid motions around the vortices*

Figure 3 shows the *rotating*-frame stream-function field associated with an equilibrium configuration of four vortices. It was discovered that there exist many distinct regions of circulating fluid separated by streamlines having at least one corner (a point where the total velocity vanishes – in the rotating frame). Figure 3 clearly shows distinct circulating regions, but we decided to examine qualitatively all of the possible regions by calculating the separating streamlines in the limit of point vortices ($a_0 \to 1$). Figures 4(*a–e*) illustrate the results for 2–6 vortices. There are five possible regions of circulating fluid: (1) central (not present for two vortices only), (2) vortex (the region around the vortex as well as the vortex itself), (3) band, (4) umbrella and (5) outer flow. Note that the band region wraps around to the inside of the vortices for

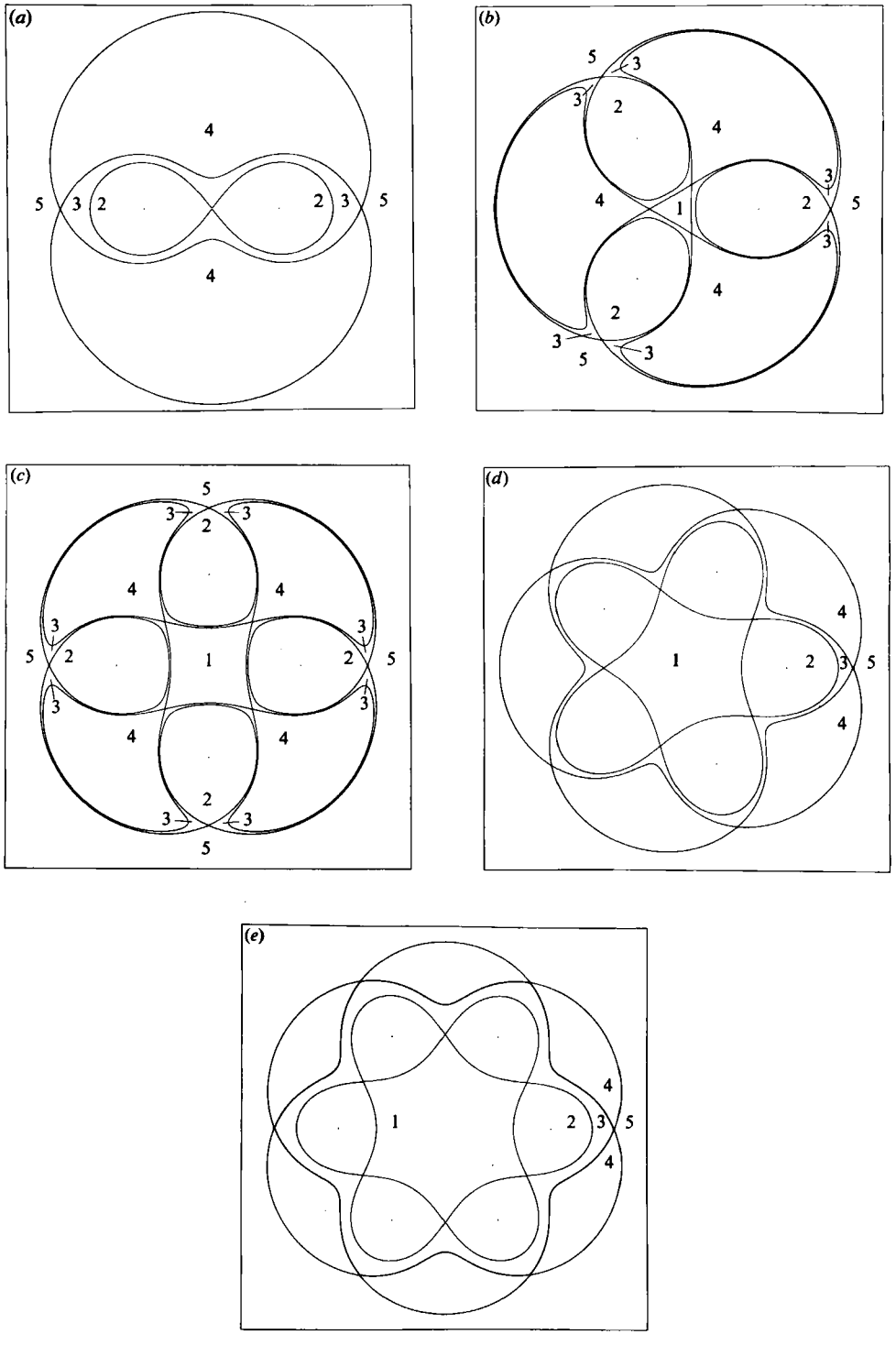

FIGURE 4. The closed circulation regions for 2–6 point vortices: (1) central, (2) vortex, (3) band, (4) umbrella and (5) outer flow. The dots indicate the vortex locations.

TABLE 1

	area/πR^2		centroid/r_0		T/T_{pv}				
a_0	exact	approx.	exact	approx.	exact	approx.	T/T^*_{pv}	$\hat{A}$	$\hat{E}$
				(*a*) 2 vortices					
0.975	0.9999	0.9999	1.0000	1.0000	1.0001	1.0001	1.0000	0.0002	9.2403
0.95	0.9997	0.9997	1.0000	1.0000	1.0003	1.0003	1.0000	0.0007	7.8284
0.9	0.9986	0.9986	1.0000	1.0000	1.0014	1.0014	1.0000	0.0028	6.3931
0.8	0.9938	0.9938	1.0000	1.0000	1.0062	1.0062	1.0000	0.0122	4.9129
0.7	0.9843	0.9839	1.0001	1.0001	1.0160	1.0156	0.9999	0.0302	4.0157
0.6	0.9681	0.9668	1.0002	1.0002	1.0329	1.0313	0.9995	0.0587	3.3653
0.5	0.9425	0.9383	1.0008	1.0008	1.0611	1.0556	0.9984	0.0994	2.8608
0.4	0.9029	0.8913	1.0022	1.0021	1.1076	1.0918	0.9957	0.1525	2.4622
0.3	0.8427	0.8130	1.0055	1.0053	1.1870	1.1450	0.9893	0.2153	2.1548
0.2	0.7522	0.6790	1.0136	1.0123	1.3321	1.2222	0.9753	0.2784	1.9397
0.1	0.6224	0.4412	1.0350	1.0280	1.6307	1.3347	0.9474	0.3201	1.8323
0.085	0.5997	0.3915	1.0408	1.0316	1.7013	1.3556	0.9418	0.3225	1.8270
0.08	0.5921	0.3739	1.0431	1.0329	1.7270	1.3628	0.9399	0.3231	1.8259
0.07	0.5767	0.3369	1.0479	1.0357	1.7823	1.3777	0.9360	0.3236	1.8246
0.065	0.5690	0.3176	1.0506	1.0371	1.8119	1.3854	0.9340	0.3237	1.8244
0.06	0.5613	0.2976	1.0535	1.0387	1.8429	1.3932	0.9321	0.3237	1.8245
0.05	0.5461	0.2557	1.0599	1.0419	1.9096	1.4094	0.9282	0.3231	1.8256
0.015	0.4970	0.0857	1.0910	1.0554	2.1963	1.4709	0.9171	0.3183	1.8358
				(*b*) 3 vortices					
0.975	0.9999	0.9999	1.0000	1.0000	1.0001	1.0001	1.0000	0.0002	6.0817
0.95	0.9996	0.9996	1.0000	1.0000	1.0004	1.0004	1.0000	0.0010	5.1407
0.9	0.9981	0.9981	1.0000	1.0000	1.0019	1.0018	1.0000	0.0041	4.1848
0.8	0.9917	0.9916	1.0000	1.0000	1.0084	1.0082	1.0000	0.0183	3.2022
0.7	0.9787	0.9784	1.0000	1.0000	1.0217	1.0208	0.9999	0.0450	2.6123
0.6	0.9559	0.9549	1.0000	1.0000	1.0456	1.0417	0.9995	0.0870	2.1924
0.5	0.9181	0.9150	1.0000	1.0000	1.0875	1.0741	0.9985	0.1456	1.8772
0.4	0.8556	0.8476	0.9999	1.0000	1.1639	1.1224	0.9958	0.2184	1.6430
0.3	0.7523	0.7320	1.0000	1.0000	1.3144	1.1933	0.9889	0.2938	1.4859
0.2	0.5896	0.5281	1.0016	1.0000	1.6558	1.2963	0.9732	0.3407	1.4162
0.185	0.5598	0.4858	1.0025	1.0000	1.7405	1.3153	0.9696	0.3420	1.4145
0.18	0.5496	0.4708	1.0028	1.0000	1.7717	1.3219	0.9684	0.3420	1.4145
0.1	0.3831	0.1554	1.0238	1.0000	2.5831	1.4463	0.9422	0.3096	1.4498
0.05	0.3254	−0.1414	1.0811	1.0000	3.3632	1.5457	0.9364	0.2874	1.4732
0.045	0.3229	−0.1768	1.0884	1.0000	3.4354	1.5568	0.9364	0.2872	1.4734
0.04	0.3207	−0.2134	1.0956	1.0000	3.5054	1.5680	0.9366	0.2874	1.4733
0.035	0.3188	−0.2513	1.1028	1.0000	3.5729	1.5795	0.9366	0.2879	1.4729

TABLE 1 (*cont.*)

	area/πR^2		centroid/r_0		T/T_{pv}				
a_0	exact	approx.	exact	approx.	exact	approx.	T/T^*_{pv}	$\hat{A}$	$\hat{E}$
				(*c*) 4 vortices					
0.975	0.9999	0.9999	1.0000	1.0000	1.0001	1.0001	1.0000	0.0003	4.6201
0.95	0.9997	0.9997	1.0000	1.0000	1.0003	1.0003	1.0000	0.0013	3.9145
0.9	0.9986	0.9986	1.0000	1.0000	1.0014	1.0014	1.0000	0.0055	3.1979
0.8	0.9937	0.9938	1.0000	1.0000	1.0063	1.0062	1.0000	0.0244	2.4626
0.7	0.9835	0.9839	0.9998	0.9998	1.0163	1.0156	1.0000	0.0604	2.0232
0.6	0.9648	0.9668	0.9992	0.9993	1.0346	1.0313	0.9998	0.1173	1.7131
0.5	0.9297	0.9383	0.9972	0.9977	1.0688	1.0556	0.9993	0.1975	1.4841
0.4	0.8570	0.8913	0.9916	0.9937	1.1444	1.0918	0.9974	0.2961	1.3222
0.3	0.6933	0.8130	0.9783	0.9842	1.3683	1.1450	0.9911	0.3772	1.2375
0.270	0.6181	0.7802	0.9722	0.9795	1.5101	1.1652	0.9875	0.3849	1.2313
0.265	0.6044	0.7742	0.9710	0.9786	1.5395	1.1688	0.9868	0.3850	1.2313
0.205	0.3992	0.6876	0.9362	0.9645	2.1401	1.2176	0.9747	0.3461	1.2586
				(*d*) 5 vortices					
0.975	1.0000	1.0000	1.0000	1.0000	1.0000	1.0000	1.0000	0.0004	3.7947
0.95	1.0000	1.0000	1.0000	1.0000	1.0000	1.0000	1.0000	0.0016	3.2303
0.9	1.0000	1.0000	1.0000	1.0000	1.0000	1.0000	1.0000	0.0069	2.6570
0.8	1.0001	1.0002	0.9999	0.9999	0.9998	1.0000	1.0000	0.0307	2.0687
0.7	1.0005	1.0016	0.9995	0.9995	0.9984	1.0000	1.0000	0.0768	1.7167
0.6	1.0024	1.0063	0.9976	0.9980	0.9927	1.0000	0.9999	0.1526	1.4669
0.5	1.0094	1.0198	0.9901	0.9938	0.9705	1.0000	0.9994	0.2780	1.2692
0.44	1.0375	1.0366	0.9711	0.9886	0.9063	1.0000	0.9970	0.3836	1.1776
				(*e*) 6 vortices					
0.975	1.0001	1.0001	1.0000	1.0000	0.9999	0.9999	1.0000	0.0005	3.2716
0.95	1.0006	1.0006	1.0000	1.0000	0.9994	0.9995	1.0000	0.0020	2.8014
0.9	1.0024	1.0024	1.0000	1.0000	0.9976	0.9977	1.0000	0.0083	2.3234
0.8	1.0113	1.0113	0.9998	0.9999	0.9885	0.9897	1.0000	0.0372	1.8319
0.7	1.0336	1.0324	0.9989	0.9991	0.9653	0.9740	0.9999	0.0952	1.5352
0.6	1.1024	1.0779	0.9940	0.9963	0.8955	0.9479	0.9991	0.2021	1.3154
0.565	1.2059	1.1038	0.9867	0.9944	0.8051	0.9356	0.9971	0.2737	1.2362
				(*f*) 7 vortices					
0.975	1.0003	1.0003	1.0000	1.0000	0.9997	0.9997	1.0000	0.0006	2.9143
0.95	1.0013	1.0013	1.0000	1.0000	0.9987	0.9987	1.0000	0.0023	2.5110
0.9	1.0057	1.0057	1.0000	1.0000	0.9943	0.9945	1.0000	0.0097	2.1009
0.8	1.0280	1.0271	0.9997	0.9998	0.9722	0.9753	0.9999	0.0442	1.6774
0.7	1.0925	1.0778	0.9980	0.9985	0.9112	0.9377	0.9994	0.1175	1.4164
0.65	1.1916	1.1224	0.9944	0.9970	0.8282	0.9100	0.9980	0.1847	1.3051

three and four vortices, but remains to the outside for all other numbers. However, for three large vortices ($a_0 = 0.1$) we have determined that the band is to the outside of the vortices. This implies that there exists a value of a_0 for which the band region is absent.

4.3. *Comparison of the exact and approximate solutions*

We now compare the exact solutions with the approximate $O(\delta^4)$ ones. Area is divided by πR^2, centroid ($x_c \equiv \iint x\,dx\,dy / \iint dx\,dy$) by r_0, and period of rotation T by $T_{pv} = 2\pi/\Omega_{pv}$, where $\Omega_{pv} = \Omega_0 = \frac{1}{4}(N-1)\,\delta^2$ is just the leading term in the perturbation expansion for small vortices. Tables 1 (*a–f*) show $A/\pi R^2$, x_c/r_0 and T/T_{pv} versus a_0 for both the exact solutions and the $O(\delta^4)$ approximate ones. Close agreement is found for small vortices. The lack of the $O(\delta^3)$ term for three vortices is evident from the x_c/r_0 column. Also, five vortices show the lack of the $O(\delta^2)$ term because $A/\pi R^2$ remains close to 1 for all a_0, differing by 3.75 % in the worst case ($a_0 = 0.44$). Other global properties of these solutions will be discussed in §10.

Finally, we point out an excellent approximation to the exact rotation period T. This is based upon point-vortex ideas. N point vortices each of strength Γ all corotate on a circle of radius x_c at a rate

$$\Omega^*_{pv} = \frac{(N-1)\,\Gamma}{4\pi x_c^2} \tag{4.1}$$

(Thomson 1883, p. 97). For finite vortices we replace Γ by A, the area of one vortex, and x_c is computed from the exact solutions. Then $T^*_{pv} \equiv 2\pi/\Omega^*_{pv}$ and the third to the last column in tables 1 (*a–f*) shows T/T^*_{pv}. The true period differs little from T^*_{pv}. In the worst case ($N = 2$, $a_0 = 0.015$), $T/T^*_{pv} = 0.9171$.

5. Stability: setting up the problem

Thomson's (1883) stability calculation for point vortices determined whether or not a slightly displaced configuration would remain near the equilibrium configuration. Six or fewer vortices are stable; seven vortices are neutrally stable even though Thomson erroneously concluded that they are slightly unstable because his calculation was not carried out to sufficient accuracy (see Morikawa & Swenson 1971). Eight or more vortices are always unstable; locally the configuration begins to look like an infinite street of vortices, which is unstable (Lamb 1932, p. 224).

Since the vortices have finite size in the present study, new instabilities may arise from the deformation of the boundaries. We set out to describe a method whereby the stability of boundary disturbances can be determined. Let $g_0(\theta)$ be the basic state as described in the previous sections. The disturbed boundary of the kth vortex ($k = 1, 2, \ldots, N$) is

$$g_k(\theta) = g_0(\theta) + g'_k(\theta, t), \tag{5.1}$$

where the perturbation $g'_k(\theta, t)$ is assumed to be a normal mode:

$$g'_k(\theta, t) = \hat{g}_k(\theta)\,e^{\sigma t}. \tag{5.2}$$

The real part of σ is the growth rate, while the imaginary part is the frequency of the boundary waves. The form of $\hat{g}_k(\theta)$ is chosen (arbitrarily) as

$$\hat{g}_k(\theta) = g_0(\theta) \sum_{m=1}^{M} C_m{}^k\,\phi_m(\theta), \tag{5.3}$$

where the ϕ_m are the orthonormal functions

$$\pi^{\frac{1}{2}}\boldsymbol{\phi} = \left(\frac{1}{\sqrt{2}}, \cos\theta, \cos 2\theta, \ldots, \cos P\theta, \sin\theta, \sin 2\theta, \ldots, \sin P\theta\right) \tag{5.4}$$

($M = 2P+1$). ${C_m}^k$ are coefficients to be determined. M is the order of truncation; the numerically computed solutions are presumed to approach the true solution as $M \to \infty$.

A point on the boundary of one perturbed vortex moves with the local fluid velocity due to all of the perturbed vortices. Thus

$$\left.\begin{aligned} \frac{\mathrm{D}g_k}{\mathrm{D}t} &= \tilde{u}_{rk} \\ \text{or} \qquad \frac{\partial g_k}{\partial t} + \frac{\tilde{u}_{\theta k}}{g_k}\frac{\partial g_k}{\partial \theta} &= \tilde{u}_{rk}, \end{aligned}\right\} \tag{5.5}$$

where $\tilde{u}_{\theta k}$ and $\tilde{u}_{rk}$ are the tangential and radial velocities relative to the 'centre' of the kth vortex, $(r_0 c_k, r_0 s_k)$, in the rotating frame (rotating at the rate Ω). Here

$$r_0 \equiv \tfrac{1}{2}(1+a_0), \quad c_k \equiv \cos(2\pi k/N), \quad \text{and} \quad s_k \equiv \sin(2\pi k/N).$$

We linearize (5.5) by substituting

$$\left.\begin{aligned} g_k(\theta, t) &= g_0(\theta) + \hat{g}_k(\theta)\, \mathrm{e}^{\sigma t}, \\ \tilde{u}_{\theta k}(\theta, t) &= \tilde{u}_{\theta 0}(\theta) + \hat{u}_{\theta k}(\theta)\, \mathrm{e}^{\sigma t}, \\ \tilde{u}_{rk}(\theta, t) &= \tilde{u}_{r0}(\theta) + \hat{u}_{rk}(\theta)\, \mathrm{e}^{\sigma t}. \end{aligned}\right\} \tag{5.6}$$

The k-independent zero-order equation is

$$\frac{1}{g_0}\frac{\mathrm{d}g_0}{\mathrm{d}\theta} = \frac{\tilde{u}_{r0}}{\tilde{u}_{\theta 0}}, \tag{5.7}$$

which, by definition, is satisfied by the basic state. The first-order equation is

$$\sigma\hat{g}_k - \frac{\tilde{u}_{\theta 0}}{g_0^2}\frac{\mathrm{d}g_0}{\mathrm{d}\theta}\hat{g}_k + \frac{\tilde{u}_{\theta 0}}{g_0}\frac{\mathrm{d}\hat{g}_k}{\mathrm{d}\theta} + \frac{1}{g_0}\frac{\mathrm{d}g_0}{\mathrm{d}\theta}\hat{u}_{\theta k} = \hat{u}_{rk}. \tag{5.8}$$

$\hat{u}_{\theta k}$ and $\hat{u}_{rk}$ are linear functionals of $\hat{g}_j$, $j = 1, 2, \ldots, N$. An expression for them is derived next. Let $\boldsymbol{u}$ be the velocity in the non-rotating frame and $\tilde{\boldsymbol{u}}$ be that in the rotating frame. Then

$$\tilde{\boldsymbol{u}}(\boldsymbol{x}) = \boldsymbol{u}(\boldsymbol{x}) + \Omega(y, -x). \tag{5.9}$$

And, with $\theta_k \equiv 2\pi k/N$,

$$\left.\begin{aligned} \tilde{u}_{\theta k} &= \tilde{v}_k \cos(\theta+\theta_k) - \tilde{u}_k \sin(\theta+\theta_k), \\ \tilde{u}_{rk} &= \tilde{u}_k \cos(\theta+\theta_k) + \tilde{v}_k \sin(\theta+\theta_k), \end{aligned}\right\} \tag{5.10}$$

where $(\tilde{u}_k, \tilde{v}_k)$ is the velocity of a point on the kth vortex's boundary. Then $\hat{u}_{\theta k}$ and $\hat{u}_{rk}$ can be obtained from the linearized versions of $\tilde{u}_{\theta k} - \tilde{u}_{\theta 0}$ and $\tilde{u}_{rk} - \tilde{u}_{r0}$ respectively. Let $\hat{\boldsymbol{u}}_k \equiv \tilde{\boldsymbol{u}}_k - \tilde{\boldsymbol{u}}_{0k}$. Then to first order

$$\begin{aligned} \hat{\boldsymbol{u}}_k = {} & \frac{1}{2\pi}\sum_{j=1}^{N}\int_0^{2\pi} \hat{g}_j(\alpha)\,\frac{(\mathrm{d}X_{0j}/\mathrm{d}\alpha)\sin(\alpha+\theta_j) - (\mathrm{d}Y_{0j}/\mathrm{d}\alpha)\cos(\alpha+\theta_j)}{r_{0kj}^2}\,(y_{0kj}, -x_{0kj})\,\mathrm{d}\alpha \\ & - \frac{\hat{g}_k(\theta)}{2\pi}\sum_{j=1}^{N}\int_0^{2\pi}\frac{(\mathrm{d}X_{0j}/\mathrm{d}\alpha)\sin(\theta+\theta_k) - (\mathrm{d}Y_{0j}/\mathrm{d}\alpha)\cos(\theta+\theta_k)}{r_{0kj}^2}\,(y_{0kj}, -x_{0kj})\,\mathrm{d}\alpha \\ & - \Omega\hat{g}_k(\theta)\,(-\sin(\theta+\theta_k), \cos(\theta+\theta_k)), \end{aligned} \tag{5.11}$$

where $\hat{\boldsymbol{u}}_k = \hat{\boldsymbol{u}}_k(\boldsymbol{x}_k)$ and

$$\boldsymbol{x}_k = (r_0 c_k + g_k(\theta, t)\cos(\theta+\theta_k),\ r_0 s_k + g_k(\theta,t)\sin(\theta+\theta_k)),$$

$$\boldsymbol{x}_{0k} = (r_0 c_k + g_0(\theta)\cos(\theta+\theta_k),\ r_0 s_k + g_0(\theta)\sin(\theta+\theta_k)),$$

$$\boldsymbol{X}_{0j} = (r_0 c_j + g_0(\alpha)\cos(\alpha+\theta_j),\ r_0 s_j + g_0(\alpha)\sin(\alpha+\theta_j)),$$

$$\boldsymbol{x}_{0kj} = \boldsymbol{x}_{0k} - \boldsymbol{X}_{0j},$$

$$r_{0kj}^2 = x_{0kj}^2 + y_{0kj}^2.$$

From this expression for $\hat{\boldsymbol{u}}_k$, $\hat{u}_{\theta k}$ and $\hat{u}_{rk}$ can be found directly from (5.10) and then substituted into the linear disturbance equation (5.8). We next replace $g_j(\alpha)$ and $g_k(\theta)$ by their equivalent sums in (5.3) and apply a Galerkin method described in Appendix A to obtain finally the eigenvalue problem

$$\sigma \boldsymbol{C}^j = \sum_{k=1}^{N} \boldsymbol{A}^{kj} \boldsymbol{C}^k, \quad j = 1, \ldots, N, \tag{5.12}$$

where $\boldsymbol{C}^j$ is the vector $(C_1^j, C_2^j, \ldots, C_M^j)$ and $\boldsymbol{A}^{kj}$ is a real $M \times M$ matrix for each k and j.

Lastly, two constraints are imposed to restrict the class of perturbations. The first keeps the area of each vortex constant so that the strength of each vortex is not changed. The second conserves the second moment (or angular momentum):

$$J = \iint \omega(x^2+y^2)\,\mathrm{d}x\,\mathrm{d}y. \tag{5.13}$$

This quantity is conserved in an inviscid fluid (see §9 for a proof) and Thomson (1883, p. 98) imposes this constraint as well. Appendix A shows how these constraints are imposed on the eigenvalue problem.

6. Stability: symmetry properties

Because of the symmetric distribution of vortices, (5.12) can be considerably simplified. The matrix $\boldsymbol{A}^{jk}$ can be thought of as an interaction matrix between the jth and kth vortices. It must depend purely upon the *relative* positions of the jth and kth vortices. This gives the symmetry property

$$\boldsymbol{A}^{jk} = \boldsymbol{A}^{j+l,\,k+l}, \quad l = 1, 2, \ldots, N, \text{ for all } j \text{ and } k. \tag{6.1}$$

This property has been confirmed by actually computing all of the $\boldsymbol{A}^{jk}$. Given $\boldsymbol{A}^{1k}$, $k = 1, \ldots, N$, all of the other $\boldsymbol{A}^{jk}$ can be found by the symmetry property above. But this is not the real advantage of recognizing this symmetry; (5.12) can be reduced to N smaller ($M \times M$) eigenvalue problems at great savings in computational expense.

Consider the case for three vortices ($N = 3$). Let $\boldsymbol{E} = \boldsymbol{A}^{11}$, $\boldsymbol{F} = \boldsymbol{A}^{12}$ and $\boldsymbol{G} = \boldsymbol{A}^{13}$. Then the complete interaction matrix is

$$\boldsymbol{A} = \begin{bmatrix} \boldsymbol{E} & \boldsymbol{F} & \boldsymbol{G} \\ \boldsymbol{G} & \boldsymbol{E} & \boldsymbol{F} \\ \boldsymbol{F} & \boldsymbol{G} & \boldsymbol{E} \end{bmatrix}, \tag{6.2}$$

and (5.12) can be separated as

$$\boldsymbol{E}\boldsymbol{C}^1 + \boldsymbol{F}\boldsymbol{C}^2 + \boldsymbol{G}\boldsymbol{C}^3 = \sigma \boldsymbol{C}^1, \tag{6.3a}$$

$$\boldsymbol{G}\boldsymbol{C}^1 + \boldsymbol{E}\boldsymbol{C}^2 + \boldsymbol{F}\boldsymbol{C}^3 = \sigma \boldsymbol{C}^2, \tag{6.3b}$$

$$\boldsymbol{F}\boldsymbol{C}^1 + \boldsymbol{G}\boldsymbol{C}^2 + \boldsymbol{E}\boldsymbol{C}^3 = \sigma \boldsymbol{C}^3. \tag{6.3c}$$

Multiply (6.3*a*) by α, (6.3*b*) by β, and (6.3*c*) by γ (α, β and γ are constants) and add:

$$(\alpha \boldsymbol{E}+\beta \boldsymbol{G}+\gamma \boldsymbol{F})\, \boldsymbol{C}^1+(\alpha \boldsymbol{F}+\beta \boldsymbol{E}+\gamma \boldsymbol{G})\, \boldsymbol{C}^2+(\alpha \boldsymbol{G}+\beta \boldsymbol{F}+\gamma \boldsymbol{E})\, \boldsymbol{C}^3 = \sigma(\alpha \boldsymbol{C}^1+\beta \boldsymbol{C}^2+\gamma \boldsymbol{C}^3). \tag{6.4}$$

Define $\boldsymbol{w} = \alpha \boldsymbol{C}^1+\beta \boldsymbol{C}^2+\gamma \boldsymbol{C}^3$. We choose (α, β, γ) such that an equation of the form

$$\boldsymbol{D}\boldsymbol{w} = \sigma \boldsymbol{w} \tag{6.5}$$

results. Then $\boldsymbol{D}$ must have the form

$$\boldsymbol{D} = \boldsymbol{E}+\frac{\beta}{\alpha}\boldsymbol{G}+\frac{\gamma}{\alpha}\boldsymbol{F} = \frac{\alpha}{\beta}\boldsymbol{F}+\boldsymbol{E}+\frac{\gamma}{\beta}\boldsymbol{G} = \frac{\alpha}{\gamma}\boldsymbol{G}+\frac{\beta}{\gamma}\boldsymbol{F}+\boldsymbol{E}, \tag{6.6}$$

so that $\alpha/\beta = \beta/\gamma = \gamma/\alpha$. There are $N = 3$ solution triplets (α, β, γ): $(1, 1, 1)$, $(1, \omega, \omega^2)$ and $(1, \omega^2, \omega^4)$, where $\omega = -\frac{1}{2}+\mathrm{i}\frac{1}{2}\sqrt{3}$, $\omega^2 = -\frac{1}{2}-\mathrm{i}\frac{1}{2}\sqrt{3}$ and $\omega^3 = 1$. 1, ω and ω^2 are the three roots of unity. Let us label these solutions by l:

$$(\alpha, \beta, \gamma)_l = (1, \omega^{(l-1)}, \omega^{2(l-1)}). \tag{6.7}$$

Three distinct eigenvalue problems are the result:

$$\boldsymbol{D}_l \boldsymbol{w}_l = \sigma_l \boldsymbol{w}_l, \quad l = 1, 2, 3. \tag{6.8}$$

In general, for N vortices

$$\boldsymbol{D}_l = \sum_{k=1}^{N} \omega^{(k-1)(l-1)} \boldsymbol{A}^{1k}, \quad \boldsymbol{w}_l = \sum_{k=1}^{N} \omega^{(k-1)(l-1)} \boldsymbol{C}^k, \tag{6.9}$$

while $\omega^N = 1$ ($\omega^m = c_m+\mathrm{i}s_m = \cos(2\pi m/N)+\mathrm{i}\sin(2\pi m/N)$).

Once the eigenvalues and eigenvectors have been found for each $\boldsymbol{D}_l$, the original eigenvectors are given by

$$\boldsymbol{C}^k = N^{-1}\omega^{-(l-1)(k-1)}\, \boldsymbol{w}_l, \quad k = 1, \ldots, N. \tag{6.10}$$

These N eigenvectors describe the disturbance (by (5.3)) on each of the N vortices. Note that, when $l = 1$, $\boldsymbol{C}^k = \boldsymbol{w}_1/N$, i.e. the disturbance is the same on each vortex. Thus l determines the symmetry of the disturbance. And, when $N = 2$ and $l = 2$, $\boldsymbol{C}^1 = -\boldsymbol{C}^2$, so the disturbance is antisymmetric.

7. Stability: numerical results

The matrix $\boldsymbol{A}$ of §5 is computed as described in Appendix A. It was truncated to $M = 21$ Galerkin functions and little change in results was seen when M was increased to 41. Routine EIGCC from the IMSL package was used to calculate the eigenvalues and eigenvectors. In this section we will look at how the eigenvalue σ depends on a_0 for $N = 2$–8 vortices and show the structure of some of the eigenmodes.

7.1. *Limiting results and stability-diagram definitions*

First let us examine the limit $a_0 \to 1$, i.e. small circular vortices. As shown in §3, the correction to this circularity is $O(\delta^2)$, where $\delta = (1-a_0)/(1+a_0)$, and this is because the influence of the other vortices is very weak. So, for small δ, the vortices behave practically independently; therefore the eigenvalues should be like those for a circular vortex (Lamb 1932, p. 230)

$$\sigma = \pm\mathrm{i}\tfrac{1}{2}(m-1), \quad m = 1, 2, \ldots. \tag{7.1}$$

The eigenfunctions consist of waves of the form $\cos(m\theta \pm \frac{1}{2}(m-1)t)$ travelling in opposite directions on each vortex's boundary. However, these waves become

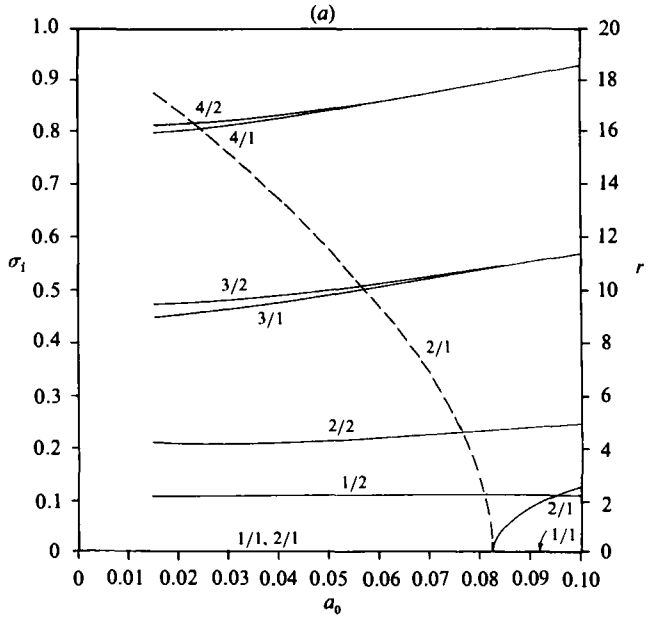

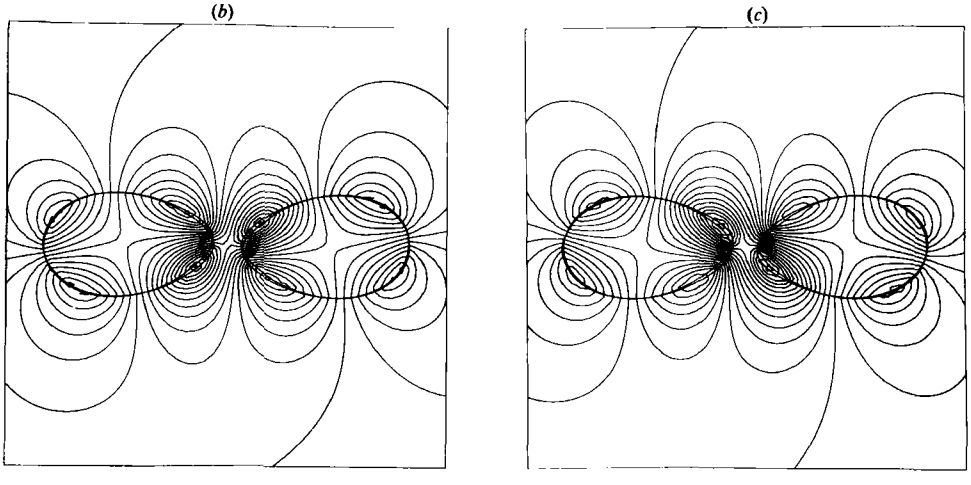

FIGURE 5. (*a*) The stability diagram for two vortices. Solid lines correspond to frequencies (σ_i) and dashed lines to growth rates ($r = \sigma_r T$). (*b*) The perturbation stream-function field (perturbed minus equilibrium) for the growing disturbance; $N = 2$, $a_0 = 0.075$, 2/1 + conjugate. (*c*) Same as in (*b*) except for the decaying counterpart.

coupled when δ increases owing to the influence of the other vortices. N different eigenmodes of N different symmetries ($l = 1, \ldots, N$, as defined in §6) become degenerate when $a_0 = 1$ for each value of m, the circular-vortex mode index. Modes on the stability diagrams to be shown in a moment will be labelled m/l, where m is the origin of the mode at $a_0 = 1$ while l indicates its symmetry.

σ ($= \sigma_r + i\sigma_i$), $-\sigma$, σ^* and $-\sigma^*$ are all eigenvalue solutions; thus only positive σ_r and σ_i will be shown. Results will be presented in terms of the quantity $r \equiv \sigma_r T$, where T is the period of rotation of the configuration ($T = 2\pi/\Omega$). Then e^r gives the amplification of the disturbance after one rotation period.

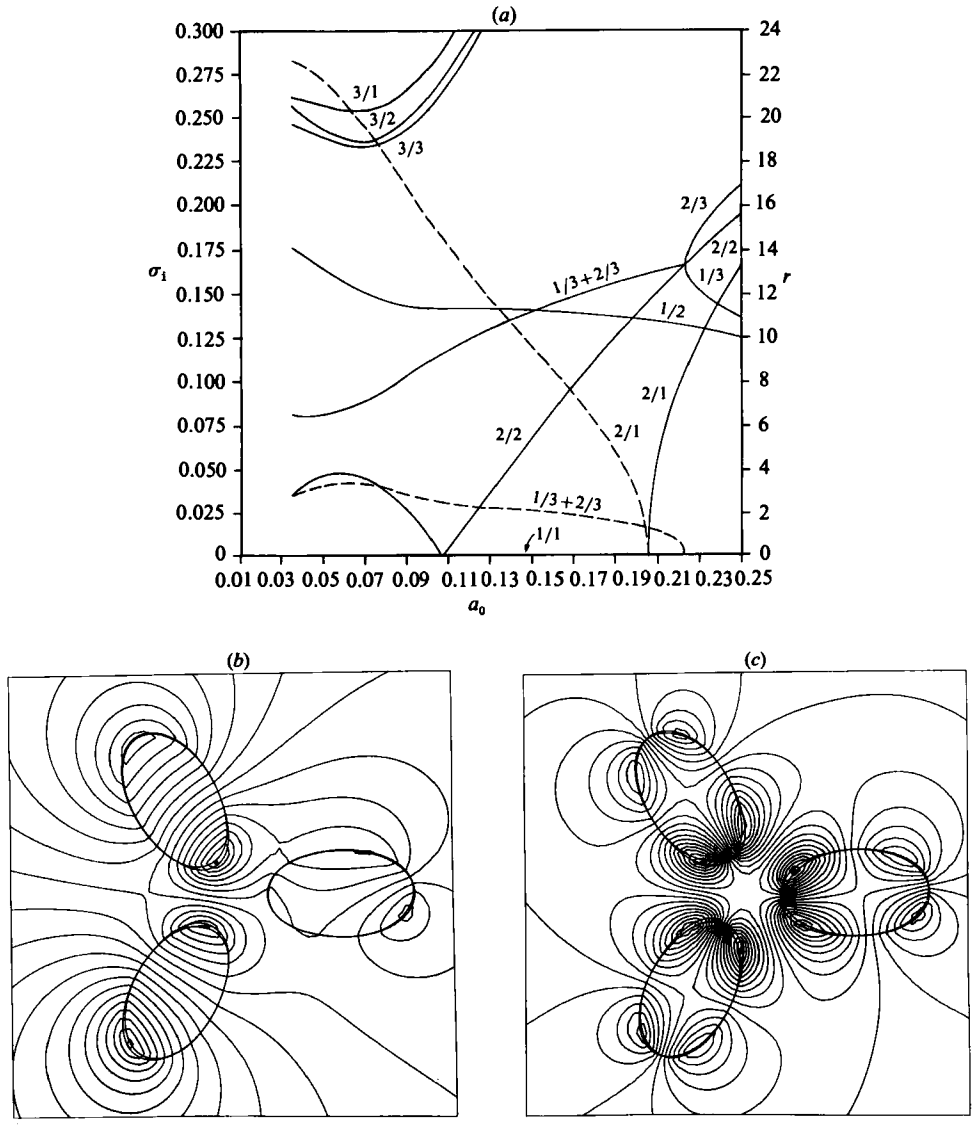

FIGURE 6. (*a*) The stability diagram for 3 vortices. The first instability is asymmetric (1/3+2/3), while a symmetric instability (2/1 + conjugate) sets in for slightly smaller a_0. (*b*) The perturbation stream-function field for the asymmetric instability; $N = 3$, $a_0 = 0.2$, 1/3+2/3. (*c*) The perturbation stream-function field for the symmetric instability; $N = 3$, $a_0 = 0.2$, 2/1 + conjugate.

7.2. *Stability diagrams for* 2–8 *vortices*

The stability diagram for two vortices is shown in figure 5 (*a*). Only the $m = 1, \ldots, 4$ mode origins are shown, and the diagram is restricted to small a_0 (large vortices) because the configuration is stable for large a_0 and m. The $m/l = 2/1$ mode coalesces with its complex conjugate at $a_0 = 0.083$, and this mode maintains zero frequency for all smaller a_0. Using an energy argument, Saffman & Szeto (1980) conjectured that the vortices would become unstable at $a_0 = 0.066$. The reasons for the discrepancy will be discussed in § 11. The growth rate of the instability rises rapidly as a_0 decreases

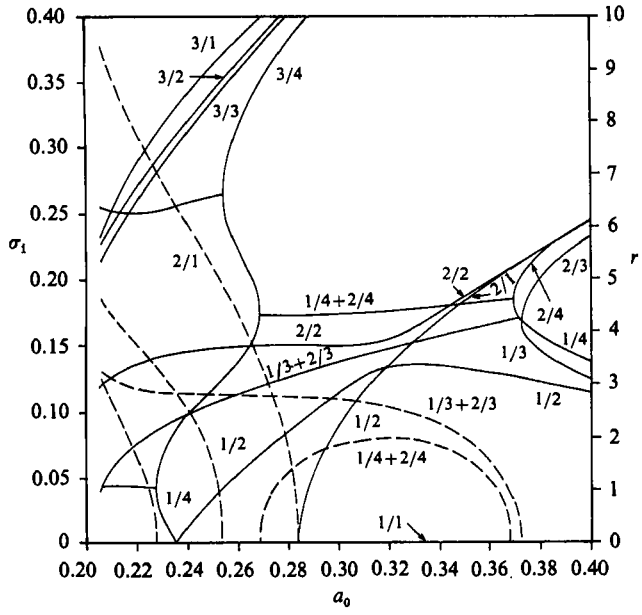

FIGURE 7. The stability diagram for 4 vortices. The first instability is antisymmetric (1/3+2/3 – every other vortex is perturbed the same way), the second is asymmetric (1/4+2/4), the third is symmetric (2/1 + conjugate), while the remaining two are asymmetric.

from 0.083. A perturbation stream-function field for the disturbance at $a_0 = 0.075$ is shown in figure 5(*b*). This diagram shows that there is a tendency for the vortices to merge. This boundary instability is unique to finite-sized vortices and is distinct from the purely displacement-type instability of Thomson's point vortices. Figure 5(*c*) contrasts with 5(*b*) by showing the decaying counterpart.

The stability of three vortices can be seen from figure 6(*a*). First, the 2/3 and 1/3 modes (asymmetric) coalesce at $a_0 = 0.223$ and remain fused for all a_0 less than this value (see figure 6*b*). At $a_0 = 0.223$, $\sigma_i \neq 0$, so that this is the onset of an *oscillatory* instability. Because of the symmetry decoupling of §4, only modes of the same l-symmetry may coalesce. Indeed the 2/1 mode (symmetric) combines with its complex conjugate at $a_0 = 0.206$ and becomes the dominant instability for $a_0 < 0.204$ (see figure 6*c*). Now, however, both σ_r and σ_i are zero at $a_0 = 0.206$. This often represents an '*exchange* of stabilities', which implies the existence of another kind of steady state (i.e. one not capable of being parametrized by a single parameter like a_0). More will be said about this in §11.

Turning next to four vortices in figure 7, we see the first instability is a result of 1/3 and 2/3 joining at $a_0 = 0.373$ and is again oscillatory. Shortly thereafter at $a_0 = 368$, 1/4 and 2/4 join but then fragment at $a_0 = 0.268$ (the growth rate vanishes there). The upper stable branch subsequently unites with the 3/4 mode at $a_0 = 0.253$ and remains intact for all smaller a_0. The 1/2 mode crosses the $\sigma_i = 0$ axis at $a_0 = 0.235$, while its mirror image, a 1/4 mode, crosses from below at the same point and then combines with the lower stable branch of the 1/4+2/4 fragmentation at $a_0 = 0.227$. Finally, the symmetric 2/1 mode merges with its conjugate at $a_0 = 0.283$, leading to an exchange of stabilities.

Five vortices are exhibited in figure 8. The stability diagram has become much simpler. The first instability occurs as 1/5 coalesces with 2/5 at $a_0 = 0.491$. Note that

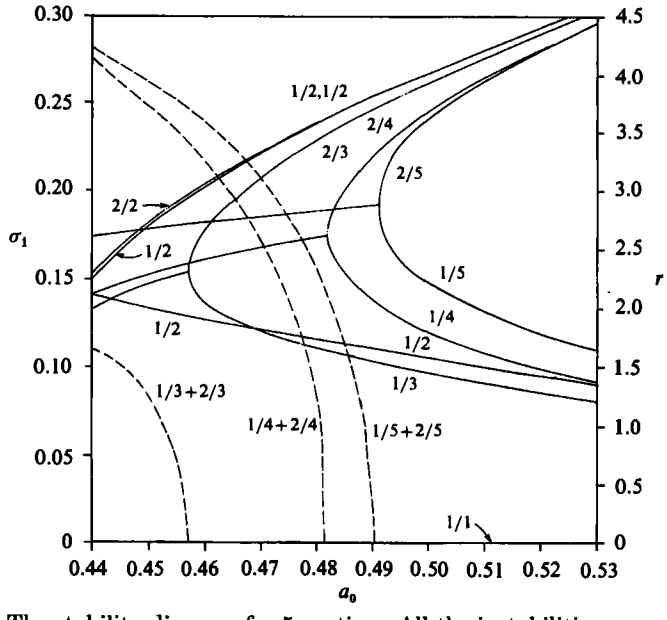

FIGURE 8. The stability diagram for 5 vortices. All the instabilities are now asymmetric.

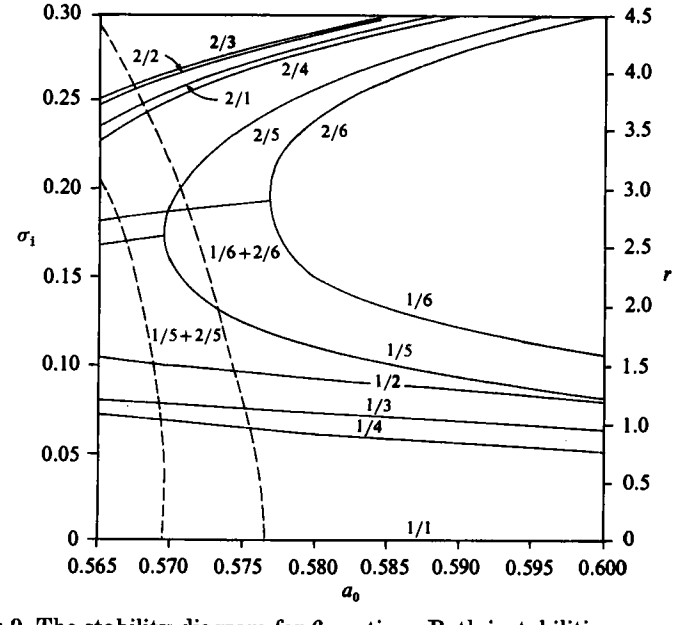

FIGURE 9. The stability diagram for 6 vortices. Both instabilities are asymmetric.

the growth rates for increasing N are decreasing. All of the unstable disturbances are now oscillatory.

Six vortices are even simpler (figure 9). 2/6 and 1/6 join at $a_0 = 0.577$ for the first instability. Again, there are no symmetric instabilities ($l = 1$), and we suspect this is true for all $N \geqslant 5$.

Seven vortices, known to be neutrally stable when $a_0 = 1$, are shown to be unstable

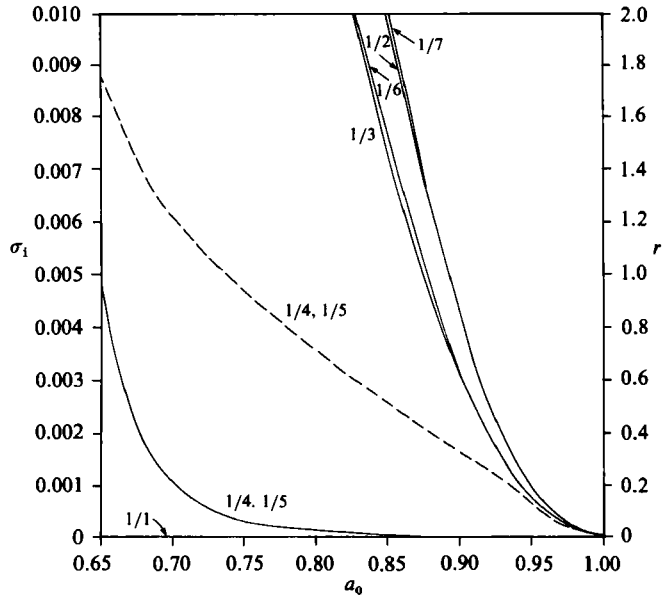

FIGURE 10. The stability diagram for 7 vortices. There are two growing displacement-like instabilities. 1/4 has a slightly higher growth rate than 1/5, and both vanish only when $a_0 = 1$ identically.

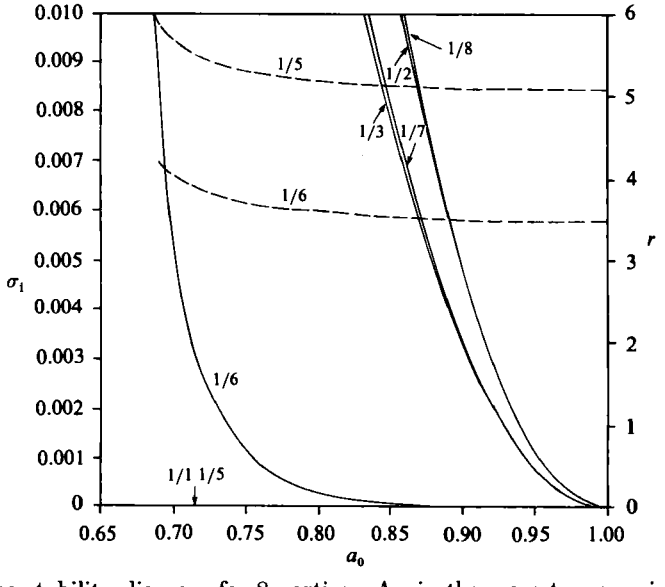

FIGURE 11. The stability diagram for 8 vortices. Again there are two growing displacement-like instabilities whose growth rates are non-zero at $a_0 = 1$, in agreement with point-vortex stability results.

for all $a_0 < 1$ (figure 10). Thus we find that the equilibrium configuration of seven point vortices is destabilized by the effects of finite size. It is the 1/4 and 1/5 modes, which account for the instability in contrast with fewer vortices. For small vortices, these ($m = 1$) modes correspond to displacing the vortices but not changing their (nearly) circular shape and thus are displacement-type instabilities. The finite size

of the vortices renders the array unstable to modes which are analogous to the displacement instabilities occurring for eight or more point vortices.

As a check on the numerical results, the stability of eight vortices was determined numerically and analytically (see Appendix B). The point-vortex stability problem is there reduced to a single formula for the growth rates:

$$\sigma_p^2 = \left(\frac{N-1}{2\pi}\right)^2 ((p-1)^2(p+1-N)^2-(N-1)^2), \quad p = 1, \ldots, N-1. \tag{7.2}$$

8 point vortices are unstable. In the finite-area case, the two displacement-type instability modes have nearly constant growth rates of 3.4763 and 5.0776 respectively in the range $0.95 < a_0 < 1$. This agrees well with the values of 3.4764 and 5.0776 predicted by (7.2). Figure 11 shows the stability diagram for eight vortices. This shows that finite size further destabilizes the vortex configuration. We expect that this holds for more than eight vortices as well, because the configuration increasingly resembles a street of vortices locally.

Thus for $N < 7$ the new modes correspond to boundary distortions, while for $N \geqslant 7$ the instabilities are just modified point-vortex modes (displacement modes).

8. Energy and excess energy of two-dimensional motion in an unbounded domain

Energy and other global properties of the fluid, if conserved, restrict the evolution of unstable, perturbed equilibrium configurations of vorticity, but, additionally, these conserved quantities determine the conditions under which an unstable initial configuration (state) may nonlinearly evolve close to a stable final or subsequent state. In the case of a viscous fluid many of the conserved quantities are lost, thus the evolutionary restrictions are considerably less severe, and much less can be said about the evolution of viscous flow. Section 9 describes in detail the conserved quantities in inviscid and viscous flow, while §10 discusses how energetics influences (nonlinear) transitions between near-equilibrium configurations. In this section we derive a new and useful energy quantity for two-dimensional motion.

In a two-dimensional fluid with non-zero total circulation the energy is infinite if the fluid is unbounded. To remove this singularity we suppose that the vorticity distribution is confined very close to the centre of a very large tank of radius L. Let l be a lengthscale characteristic of the vorticity distribution. Then we require that $l/L \ll 1$. More will be said about the choice of l in a moment.

For an infinite incompressible fluid without interior boundaries, the stream function $\psi(x, y)$ is

$$\psi = (2\pi)^{-1} \iint \omega' \log \frac{r}{L} \, dx' \, dy', \tag{8.1}$$

where $r^2 = (x'-x)^2+(y'-y)^2$ and $\omega' = \omega(x', y')$ is the vorticity distribution. The kinetic energy

$$T = \frac{1}{2} \iint (u^2+v^2) \, dx \, dy, \tag{8.2}$$

with $u = -\psi_y$ and $v = \psi_x$, approaches the 'excess energy'

$$T_e = -\frac{1}{2} \iint \omega\psi \, dx \, dy, \tag{8.3}$$

as $l/L \to 0$ (with $O(l/L)$ errors), since the boundary integral appearing in the transformation from T into T_e via Stokes' Theorem yields a vanishing contribution as $l/L \to 0$.

Introducing the following non-dimensionalization,

$$\left.\begin{aligned} \hat{x} = \frac{x}{l}, \quad \hat{y} = \frac{y}{l}, \quad \hat{r} = \frac{r}{l}, \\ \hat{\omega} = \frac{\omega l^2}{\Gamma}, \quad \hat{\psi} = \frac{\psi}{\Gamma}, \quad \hat{T} = \frac{T}{\Gamma^2}, \end{aligned}\right\} \tag{8.4}$$

where

$$\Gamma = \iint \omega \, \mathrm{d}x \, \mathrm{d}y \tag{8.5}$$

is the total circulation (a conserved quantity even in a viscous fluid – a proof will be given later), we find that $\hat{\psi}$ and $\hat{T}$ separate into L-dependent and L-independent terms:

$$\left.\begin{aligned} \hat{\psi} = (2\pi)^{-1} \log \frac{l}{L} + \hat{\psi}_s, \quad \hat{\psi}_s = (2\pi)^{-1} \iint \hat{\omega}' \log \hat{r}' \, \mathrm{d}\hat{x}' \, \mathrm{d}\hat{y}', \\ \hat{T} = -(4\pi)^{-1} \log \frac{l}{L} + \hat{T}_s, \quad \hat{T}_s = -\frac{1}{2} \iint \hat{\omega} \hat{\psi}_s \, \mathrm{d}\hat{x} \, \mathrm{d}\hat{y}. \end{aligned}\right\} \tag{8.6}$$

It will be shown in §9 that the second moment J, proportional to the angular momentum, is conserved in an inviscid fluid. J is redefined as

$$J = 2 \iint \omega(x^2 + y^2) \, \mathrm{d}x \, \mathrm{d}y, \tag{8.7}$$

and l is now chosen to be

$$l = (J/\Gamma)^{\frac{1}{2}} \tag{8.8}$$

($l = R$ for a circular constant-vorticity vortex of radius R). Then $\hat{T}$ can be rewritten as

$$\hat{T} = -(8\pi)^{-1} \log \frac{J}{\Gamma L^2} + \hat{T}_s. \tag{8.9}$$

For inviscid transitions between two near-equilibrium configurations, J and Γ are conserved while L is fixed by definition, so that all we must require is that $\hat{T}_s$ be the same for the initial and final states. We will see that this form of $\hat{T}$ is also useful in the viscous case.

Saffman & Szeto (1980) also defined an excess energy, but they used l^2 proportional to vortex area instead of J/Γ. Our formulation appears to be the most general in that it can apply to any vorticity distribution with finite circulation including vortices of different strengths and non-uniform distributions.

9. Conserved and non-conserved quantities in a viscous fluid

As stated earlier, the circulation of an unbounded viscous fluid is conserved. This is proved as follows. The vorticity equation

$$\frac{\mathrm{d}\omega}{\mathrm{d}t} = \nu \nabla^2 \omega, \tag{9.1}$$

(ν is the constant viscosity), can be used to calculate

$$\frac{\mathrm{d}\Gamma}{\mathrm{d}t} = \frac{\mathrm{d}}{\mathrm{d}t}\iint \omega \,\mathrm{d}x\,\mathrm{d}y = \iint \frac{\partial \omega}{\partial t}\,\mathrm{d}x\,\mathrm{d}y. \tag{9.2}$$

Since

$$\frac{\partial \omega}{\partial t} = -\boldsymbol{u}\cdot\boldsymbol{\nabla}\omega + \nu\nabla^2\omega \tag{9.3}$$

we have

$$\begin{aligned}\frac{\mathrm{d}\Gamma}{\mathrm{d}t} &= -\iint \boldsymbol{u}\cdot\boldsymbol{\nabla}\omega \,\mathrm{d}x\,\mathrm{d}y + \nu\iint \boldsymbol{\nabla}\cdot\boldsymbol{\nabla}\omega \,\mathrm{d}x\,\mathrm{d}y \\ &= -\iint (\boldsymbol{\nabla}\cdot(\omega\boldsymbol{u}) - \omega\,\boldsymbol{\nabla}\cdot\boldsymbol{u})\,\mathrm{d}x\,\mathrm{d}y + \nu\iint \boldsymbol{\nabla}\cdot\boldsymbol{\nabla}\omega \,\mathrm{d}x\,\mathrm{d}y \\ &= -\int_\infty \omega\boldsymbol{u}\cdot\hat{\boldsymbol{n}}\,\mathrm{d}l + \nu\int_\infty \boldsymbol{\nabla}\omega\cdot\hat{\boldsymbol{n}}\,\mathrm{d}l,\end{aligned} \tag{9.4}$$

where $\hat{\boldsymbol{n}}$ is the normal vector and $\mathrm{d}l$ is an infinitesimal displacement along the boundary at infinity (we have used Gauss' Theorem and $\boldsymbol{\nabla}\cdot\boldsymbol{u} = 0$). Because we have assumed Γ to be finite, this puts a constraint on ω as $r = (x^2+y^2)^{\frac{1}{2}} \to \infty$. Suppose $\omega \approx Cr^\alpha$ as $r\to\infty$. The part of the total circulation in the annulus $r_1 < r < r_2$ as $r_1, r_2 \to \infty$ and $r_2 \gg r_1$ is

$$\Delta\Gamma \approx \int_0^{2\pi}\mathrm{d}\theta\int_{r_1}^{r_2} r\,\mathrm{d}r(Cr^\alpha) = \frac{2\pi C}{\alpha+2}(r_2^{\alpha+2} - r_1^{\alpha+2}). \tag{9.5}$$

Thus, if Γ is to remain finite, $\alpha < -2$. This can now be used to evaluate the contour integrals in $\mathrm{d}\Gamma/\mathrm{d}t$. The normal component of the velocity is $O(J/r^3)$ as $r\to\infty$, which can be seen by considering the dipole moment of the vorticity distribution. Also, $\boldsymbol{\nabla}\omega\cdot\hat{\boldsymbol{n}} \approx r^{-1}\partial(r\omega)/\partial r \approx C(\alpha+1)\,r^{\alpha-1}$, so that (9.4) becomes

$$\begin{aligned}\frac{\mathrm{d}\Gamma}{\mathrm{d}t} &= \lim_{r\to\infty}\left[-Cr^\alpha\left(\frac{J}{r^3}\right)2\pi r + C(\alpha+1)\,r^{\alpha-1}\,2\pi r\right] \\ &\propto \lim_{r\to\infty} r^\alpha = 0.\end{aligned} \tag{9.6}$$

It can be shown in an analogous fashion that two other quantities are conserved:

$$\bar{x} = \Gamma^{-1}\iint \omega x\,\mathrm{d}x\,\mathrm{d}y \quad\text{and}\quad \bar{y} = \Gamma^{-1}\iint \omega y\,\mathrm{d}x\,\mathrm{d}y. \tag{9.7}$$

There seem to be no other conserved quantities.

For an inviscid fluid, the energy and the second moment are both conserved but this property is lost in a viscous fluid. Consider first the energy evolution. It can be shown that the dissipation of energy takes the form (Lamb 1932, p. 580)

$$\frac{\mathrm{d}T}{\mathrm{d}t} = -\tfrac{1}{2}\nu\eta = -\tfrac{1}{2}\nu\iint \omega^2\,\mathrm{d}x\,\mathrm{d}y. \tag{9.8}$$

The usual boundary integrals vanish owing to the asymptotic behaviour of ω. For the second moment (8.7) we have

$$\frac{\mathrm{d}J}{\mathrm{d}t} = \frac{\mathrm{d}}{\mathrm{d}t}\iint 2\omega(x^2+y^2)\,\mathrm{d}x\,\mathrm{d}y = 2\iint \frac{\partial\omega}{\partial t}(x^2+y^2)\,\mathrm{d}x\,\mathrm{d}y. \tag{9.9}$$

Let $f = \frac{1}{2}(x^2+y^2)$. Then

$$\frac{\mathrm{d}J}{\mathrm{d}t} = -4\iint f\,\boldsymbol{\nabla}\cdot(\omega\boldsymbol{u})\,\mathrm{d}x\,\mathrm{d}y + 4\nu\iint f\,\boldsymbol{\nabla}\cdot\boldsymbol{\nabla}\omega\,\mathrm{d}x\,\mathrm{d}y$$

$$= -4\iint (\boldsymbol{\nabla}\cdot(f\omega\boldsymbol{u}) - \omega\boldsymbol{u}\cdot\boldsymbol{x})\,\mathrm{d}x\,\mathrm{d}y + 4\nu\iint (\boldsymbol{\nabla}\cdot(f\,\boldsymbol{\nabla}\omega) - \boldsymbol{x}\cdot\boldsymbol{\nabla}\omega)\,\mathrm{d}x\,\mathrm{d}y. \quad (9.10)$$

But $\boldsymbol{x}\cdot\boldsymbol{\nabla}\omega = \boldsymbol{\nabla}\cdot(\omega\boldsymbol{x}) - 2\omega$. So

$$\frac{\mathrm{d}J}{\mathrm{d}t} = -4\int_\infty f\omega\boldsymbol{u}\cdot\hat{\boldsymbol{n}}\,\mathrm{d}l + 4\nu\int_\infty (f\,\boldsymbol{\nabla}\omega - \omega\boldsymbol{x})\cdot\hat{\boldsymbol{n}}\,\mathrm{d}l + 4\iint \omega\boldsymbol{u}\cdot\boldsymbol{x}\,\mathrm{d}x\,\mathrm{d}y + 8\nu\Gamma. \quad (9.11)$$

The first boundary integral vanishes as r^α, while the second integral vanishes as $r^{\alpha+2}$ as $r\to\infty$ ($\alpha < -2$). We next show that the term

$$\iint \omega\boldsymbol{u}\cdot\boldsymbol{x}\,\mathrm{d}x\,\mathrm{d}y \quad (9.12)$$

vanishes. Since $\nabla^2\psi = \omega$, $u = -\psi_y$ and $v = \psi_x$, we have

$$\left.\begin{aligned} \psi(\boldsymbol{x}) &= \frac{1}{2\pi}\iint \omega(\boldsymbol{x}')\log|\boldsymbol{x}-\boldsymbol{x}'|\,\mathrm{d}x'\,\mathrm{d}y', \\ u(\boldsymbol{x}) &= \frac{-1}{2\pi}\iint \omega(\boldsymbol{x}')\frac{y-y'}{|\boldsymbol{x}-\boldsymbol{x}'|^2}\,\mathrm{d}x'\,\mathrm{d}y', \\ v(\boldsymbol{x}) &= \frac{1}{2\pi}\iint \omega(\boldsymbol{x}')\frac{x-x'}{|\boldsymbol{x}-\boldsymbol{x}'|^2}\,\mathrm{d}x'\,\mathrm{d}y'. \end{aligned}\right\} \quad (9.13)$$

So

$$\iint \omega\boldsymbol{u}\cdot\boldsymbol{x}\,\mathrm{d}x\,\mathrm{d}y = \frac{1}{2\pi}\iint \mathrm{d}x\,\mathrm{d}y\iint \mathrm{d}x'\,\mathrm{d}y'\,\omega(\boldsymbol{x})\,\omega(\boldsymbol{x}')\frac{(x-x')\,y-(y-y')\,x}{|\boldsymbol{x}-\boldsymbol{x}'|^2}$$

$$= \frac{1}{2\pi}\iint \mathrm{d}x\,\mathrm{d}y\iint \mathrm{d}x'\,\mathrm{d}y'\,\omega(\boldsymbol{x})\,\omega(\boldsymbol{x}')\frac{xy'-x'y}{|\boldsymbol{x}-\boldsymbol{x}'|^2}$$

$$= 0, \quad (9.14)$$

because the primed and unprimed variables may be interchanged while the integral must be the same. Thus the surprisingly simple result is

$$\frac{\mathrm{d}J}{\mathrm{d}t} = 8\nu\Gamma, \quad (9.15)$$

a constant; hence $J(t) = J(0) + 8\nu\Gamma t$, a result first obtained by Poincaré (1893) (see also Ting 1983). When the fluid is inviscid J is conserved. Otherwise, it simply increases linearly with time. This represents the diffusion of the vorticity distribution. The fact that this result is independent of the details of the distribution is rather surprising. The physical content of (9.15) is that viscous dissipation spreads the vorticity over a progressively greater area.

10. Transitions based on energy

10.1. *Transition constraints*

We now make use of the results of §§8 and 9 to put constraints on the evolution of unstable configurations. Our purpose is twofold: first, we consider this procedure as an important step toward understanding *non*linear stability, and, secondly, it seems as though energetic constraints determine the eventual fate of an unstable configuration. With regards to the second issue, it appears possible for a perturbed configuration to evolve close to a radically different configuration. The discussion to follow suggests that such eventualities may occur. To this end, we will consider three types of evolution: (1) viscous, (2) inviscid and (3) nearly inviscid. Different evolutionary possibilities characterize the three cases.

Recall from (9.8) that the dissipation rate is given by

$$\frac{\mathrm{d}T}{\mathrm{d}t} = -\tfrac{1}{2}\nu\eta = -\tfrac{1}{2}\nu \int\int \omega^2 \,\mathrm{d}x\,\mathrm{d}y, \tag{10.1}$$

meanwhile from (9.15)

$$\frac{\mathrm{d}J}{\mathrm{d}t} = 8\nu\Gamma, \tag{10.2}$$

while Γ remains conserved. Let T_i be the initial kinetic energy and T_f be the kinetic energy of the subsequent state. Then $T_\mathrm{f} - T_\mathrm{i} \equiv \Delta T \leqslant 0$. Remember that T can be split up as (see (8.6))

$$\hat{T} = \frac{T}{\Gamma^2} = \frac{1}{8\pi}\log\frac{J}{\Gamma L^2} + \hat{T}_\mathrm{s}, \tag{10.3}$$

so that

$$\Delta\hat{T} = \frac{\Delta T}{\Gamma^2} = \frac{1}{8\pi}\log\frac{J_\mathrm{i}}{J_\mathrm{f}} + \hat{T}_\mathrm{sf} - \hat{T}_\mathrm{si}, \tag{10.4}$$

showing that $\Delta\hat{T} < 0$ can be satisfied if

$$\hat{T}_\mathrm{sf} < \hat{T}_\mathrm{si} - \frac{1}{8\pi}\log\frac{J_\mathrm{i}}{J_\mathrm{f}}. \tag{10.5}$$

Since $J_\mathrm{i}/J_\mathrm{f} \leqslant 1$ it is thus possible to have $\hat{T}_\mathrm{sf} > \hat{T}_\mathrm{si}$. All one may say about viscous evolution is that $J_\mathrm{f} > J_\mathrm{i}$ and $\Delta\hat{T} < 0$. The latter requirement implies that $\hat{T}_\mathrm{sf}$ may not exceed $\hat{T}_\mathrm{si}$ by more than $(8\pi)^{-1}\log(J_\mathrm{f}/J_\mathrm{i})$.

For inviscid transitions $J_\mathrm{f} = J_\mathrm{i}$, $\hat{T}_\mathrm{sf} = \hat{T}_\mathrm{si}$, and, in the general case of a non-uniform vorticity distribution, there would be an infinite number of other constraints because integrals of any moment of the vorticity distribution are conserved:

$$\frac{\mathrm{d}M_k}{\mathrm{d}t} = 0, \quad M_k = \int\int \omega^k \,\mathrm{d}x\,\mathrm{d}y, \quad k = 1, 2, \ldots. \tag{10.6}$$

However, for a *piecewise-constant* vorticity distribution, the M_k are given by $\Sigma_j \omega_j{}^k A_j$, where ω_j and A_j are the constant vorticity and area of the jth region. As a consequence of the local conservation of vorticity ($\mathrm{d}\omega/\mathrm{d}t = 0$) and incompressibility, the ω_j and the A_j are always conserved. Thus all the moments are automatically conserved. Then, for this simple distribution of vorticity, there appears to be only a finite number of independently conserved quantities (ω_j, A_j, $\bar{x}$, $\bar{y}$, Γ, J and $\hat{T}$). We will shortly show that this large number of conserved quantities severely restricts inviscid evolution.

When the dissipation is small there is an extra constraint not present in the case of large dissipation, but fewer constraints when compared with inviscid flow. A

'nearly' inviscid transition is one for which the non-dimensional parameter $\beta \equiv \nu \Delta t/l^2 \ll 1$, where Δt is the transition time between near-equilibrium states. Δt need not be very large – an example with moderate Δt will be presented shortly. In general, we can estimate Δt by assuming that the amplitude of the perturbation, initially ϵ, grows to $O(1)$; the time Δt this takes is approximately $\sigma_{\rm r}^{-1} \log(1/\epsilon)$, where $\sigma_{\rm r}$ is the growth rate of the linear disturbance. We derive next an equation that relates the final state to the initial state and the amount of dissipation. Define

$$\Delta \hat{J} = \frac{J_{\rm f} - J_{\rm i}}{J_{\rm i}} = \frac{J_{\rm f}}{J_{\rm i}} - 1 = 8\beta, \tag{10.7}$$

where we have used (10.2) and $l^2 = J/\Gamma$. Then

$$\Delta \hat{T} = \hat{T}_{\rm sf} - \hat{T}_{\rm si} - \frac{1}{8\pi} \log(1 + \Delta \hat{J}) \approx \hat{T}_{\rm sf} - \hat{T}_{\rm si} - \frac{\beta}{\pi}. \tag{10.8}$$

Because $\mathrm{d}T/\mathrm{d}t = -\frac{1}{2}\nu\eta$ and since η will only change by a small fraction of itself during the transition (η is conserved in inviscid flow), $\mathrm{d}T/\mathrm{d}t$ can be evaluated at the initial time:

$$\frac{\mathrm{d}T}{\mathrm{d}t} \approx -\tfrac{1}{2}\nu\eta_{\rm i}, \tag{10.9}$$

so that

$$\Delta \hat{T} \approx -\frac{\nu \eta_{\rm i} \Delta t}{2\Gamma^2} = -\beta \frac{J_{\rm i} \eta_{\rm i}}{2\Gamma^3}. \tag{10.10}$$

Upon eliminating β from the expressions for $\Delta \hat{J}$ and $\Delta \hat{T}$ we find

$$\Delta \hat{J} = -\frac{16\Gamma^3}{J_{\rm i}\eta_{\rm i}} \Delta \hat{T}. \tag{10.11}$$

So (10.8) becomes

$$\Delta \hat{T} \approx \hat{T}_{\rm sf} - \hat{T}_{\rm si} + \frac{2\Gamma^3}{\pi J_{\rm i}\eta_{\rm i}} \Delta \hat{T}, \tag{10.12}$$

or, rearranging,

$$\hat{T}_{\rm sf} = \hat{T}_{\rm si} + \Delta \hat{T}\left(1 - \frac{2\Gamma^3}{\pi J_{\rm i}\eta_{\rm i}}\right). \tag{10.13}$$

This equation relates the *structures* but not the lengthscales of the initial and final configurations. The lengthscale $l_{\rm i} = (J_{\rm i}/\Gamma)^{\frac{1}{2}}$ and $l_{\rm f} = (J_{\rm f}/\Gamma)^{\frac{1}{2}}$ are related by (10.7):

$$l_{\rm f}/l_{\rm i} \approx 1 + 4\beta, \tag{10.14}$$

so that the lengthscale of the final state is always largest. In general (for an arbitrary non-uniform vorticity distribution) there are an extra infinite number of equations of the form (10.13) (because of (10.6)), but none of these can be put in such a simple form. If from (10.13) one can find an initial and final state for a given small $\Delta \hat{T}$, one must make sure that the fractional change of the other approximately conserved quantities are all $\ll 1$. This is a consistency check. Summarizing then, in the case of small dissipation, (10.11) represents an additional constraint not present in the case of large dissipation, where $\Delta \hat{T}$ and $\Delta \hat{J}$ are unrelated.

For constant-vorticity vortices, the situation appears considerably simpler because the only additional almost-conserved quantity is the vortex area. We would like to write down an equation analogous to (10.13) to express near-conservation of area, but this has so far proved impossible. Furthermore, vortex area only makes sense for a piecewise-constant vorticity distribution that evolves inviscidly. In order to

extend the concept of vortex area to non-uniform vorticity distributions, first notice that, for the N corotating vortices of this study, the quantity

$$\hat{A} = \frac{NA}{\pi l^2} \tag{10.15}$$

represents the non-dimensional area (divided by π) of the whole configuration. Here A is the dimensional area of one vortex and $l^2 = J/\Gamma$ as before. The quantity appearing in (10.13), $\Gamma^3/\pi J_i \eta_i$, is just $\hat{A}_i$. Thus define, for a general vorticity distribution,

$$\hat{A} = \frac{\Gamma^3}{\pi J \eta}. \tag{10.16}$$

Because $\hat{A} = 1$ for a single constant-vorticity circular vortex while $\hat{T}_s = 1/16\pi$, let us define $\hat{E} \equiv 16\pi \hat{T}_s$ and $\Delta\hat{E} \equiv 16\pi\,\Delta\hat{T} = -8\beta/\hat{A}_i$. Then (10.13) can be rewritten as

$$\hat{E}_{sf} = \hat{E}_{si} + \Delta\hat{E}(1 - 2\hat{A}_i). \tag{10.17}$$

10.2. *Examples of transitions*

We next determine the specific conditions under which one unstable near-equilibrium state may become another near-equilibrium state. We first consider the transition between N_i corotating constant-vorticity vortices and N_f vortices. The initial state is characterized by a_{0i}, a_{1i}^*, and N_i vortices and the final state by a_{0f}, a_{1f}^*, and N_f vortices, where a_1^* is the lengthscale of the configuration as defined in figure 1. For an inviscid transition

$$\left.\begin{aligned} \hat{E}(a_{0i}, N_i) &= \hat{E}(a_{0f}, N_f), \\ \hat{A}(a_{0i}, N_i) &= \hat{A}(a_{0f}, N_f), \\ l(a_{0i}, a_{1i}^*, N_i) &= l(a_{0f}, a_{1f}^*, N_f). \end{aligned}\right\} \tag{10.18}$$

The last equation relates a_{1f}^* to a_{1i}^*. We have already taken into account that Γ and J are conserved. $\Gamma = \omega NA$ and ω is the constant value of the vorticity inside the vortices before and after the transition because ω cannot change without dissipation of energy. Γ-conservation implies $N_i A(a_{0i}, N_i) = N_f A(a_{0f}, N_f)$, but, because Γ and J are conserved and $l^2 = J/\Gamma$, (10.15) shows that $\hat{A}$-conservation is just a convenient non-dimensional form of Γ-conservation.

Figures 12 and 13 show $\hat{E}(a_0, N)$ and $\hat{A}(a_0, N)$ for 2–8 vortices (see also tables 1*a–f*). A curious property of these curves is that (for the same N) $\mathrm{d}\hat{E}/\mathrm{d}a_0$ and $\mathrm{d}\hat{A}/\mathrm{d}a_0$ vanish at the same values of a_0 for $N = 2$, 3 and 4 vortices. More will be said about this in §11. For the present, we note that the first equation in (10.18) can be solved for a_{0f}, say $a_{0f} = F(a_{0i})$. Meanwhile, the second can be solved similarly, say $a_{0f} = G(a_{0i})$. Consistency then requires that $F(a_{0i}) = G(a_{0i})$. However, for any combination of N_i and N_f, this equation has *no* solution. In other words, an inviscid transition cannot occur between two different configurations of corotating vortices.

So, transitions between N_i and N_f vortices, if they were to occur, must involve dissipation. The amount of dissipation can alternatively be looked upon as a measure of the incompleteness of an inviscid transition – in fact, this interpretation seems to be of the greatest practical value. In any case, we can estimate the amount of dissipation by using (10.17). Assuming *a priori* that there may be nearly inviscid (or nearly complete) transitions, the change in $\hat{A}$ will be very small; if we set $\hat{A}_f = \hat{A}_i$ just to see roughly where $|\Delta\hat{E}|$ as calculated from (10.17) is smallest, we find that the transition with the smallest $|\Delta\hat{E}|$ (when the initial state is unstable) is $N_i = 4$,

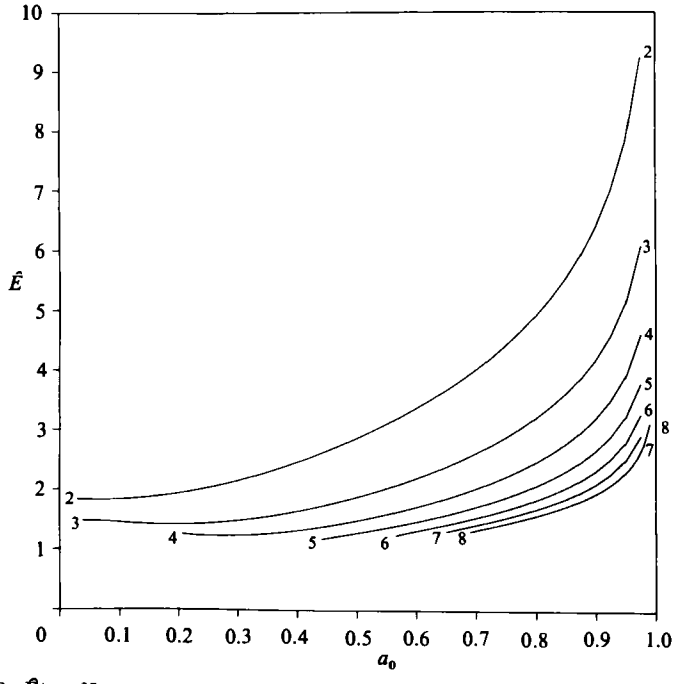

FIGURE 12. $\hat{E}(a_0, N)$ versus a_0 for $N = 2$–8 vortices. $\hat{E} = 1$ for a uniform circular vortex.

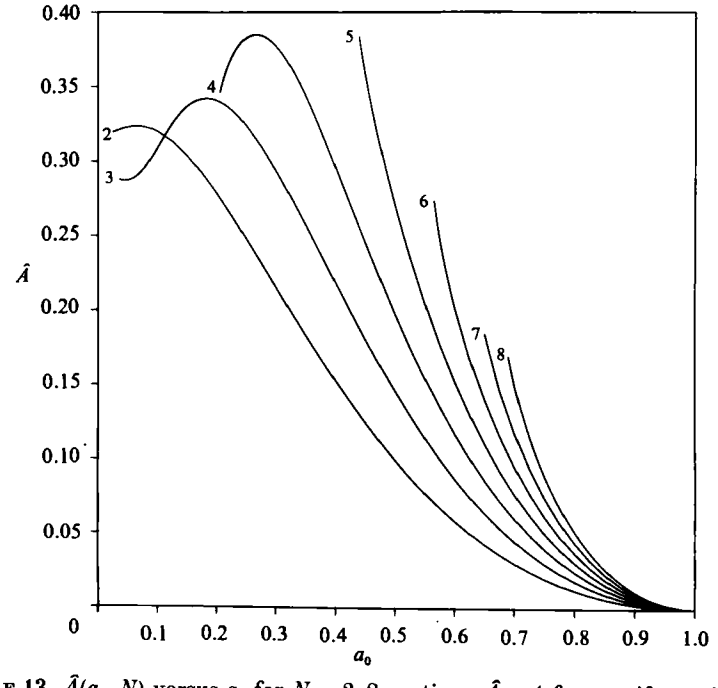

FIGURE 13. $\hat{A}(a_0, N)$ versus a_0 for $N = 2$–8 vortices. $\hat{A} = 1$ for a uniform circular vortex.

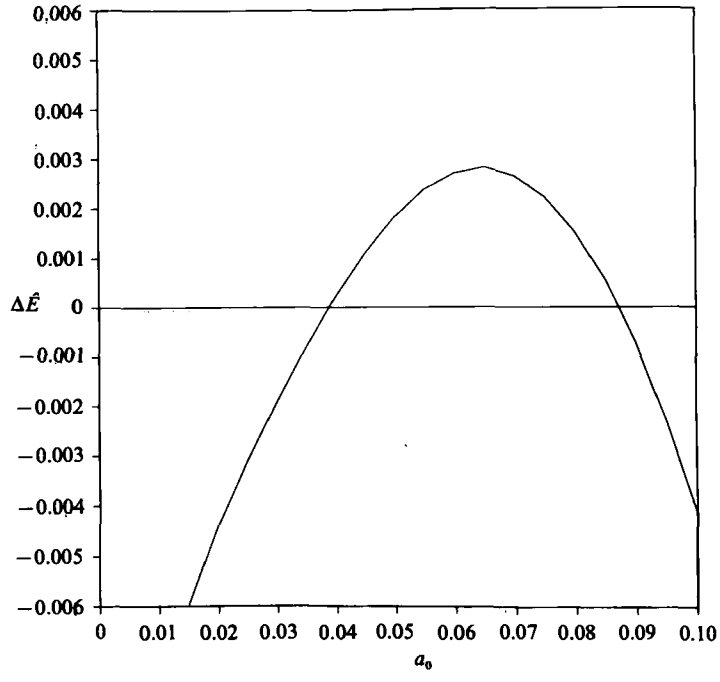

FIGURE 14. The transition dissipation $\Delta\hat{E}$ is shown for $N = 2$ vortices in the range $0 \leqslant a_0 \leqslant 0.1$. The smallness of $\Delta\hat{E}$ indicates that a nearly inviscid transition to an ellipse is possible for all unstable a_0 ($a_0 < 0.083$).

$a_{0i} = 0.373$ to $N_f = 5$, $a_{0f} = 0.47$; then $\Delta\hat{E} = -0.185$ ($\beta = 0.008$). However, the final state is itself unstable, and its subsequent evolution would involve still more dissipation. The concept of 'final state' becomes meaningless when $\beta = \nu\Delta t/l^2$ ceases to be small, because the initial configuration is expected to be markedly different owing to the smearing effects of viscosity (alternatively, one can only hope to get within $O(\beta)$ of the assumed 'final' state – see Dritschel (1985) for more details regarding actual nonlinear (inviscid) transitions). We conclude that stable near-equilibrium final states may not occur.

As a second example of these energy ideas, transitions between an elliptical vortex and the corotating vortices are sought next. The ellipse is a simple-enough equilibrium vorticity distribution to have analytic expressions for $\hat{E}$ and $\hat{A}$:

$$\left.\begin{aligned} \hat{E} &= 1 - 2\log\frac{(1+c)^2}{2(1+c^2)}, \\ \hat{A} &= \frac{2c}{1+c^2}, \end{aligned}\right\} \tag{10.19}$$

where $c = b/a$, the ratio of the semiminor to semimajor axis lengths. As with the N_i to N_f vortex transition, inviscid and nearly inviscid transitions were sought by setting $\hat{A}$(ellipse) = $\hat{A}$(N-state) to determine $c(a_0, N)$ and therefore $\hat{E}$(ellipse). Then (10.17) is solved for $\Delta\hat{E}(a_0, N)$ with $\hat{E}_i = \hat{E}$(N-state) and $\hat{E}_f = \hat{E}$(ellipse). $\Delta\hat{E}$ is shown in figure 14 for $N = 2$ vortices and $0 < a_0 < 0.1$. Recall that two vortices are unstable if $a_0 < 0.083$. What is so surprising about this figure is the smallness of $\Delta\hat{E}$ over this entire range (and β is about 25 times smaller). This suggests that an approximately

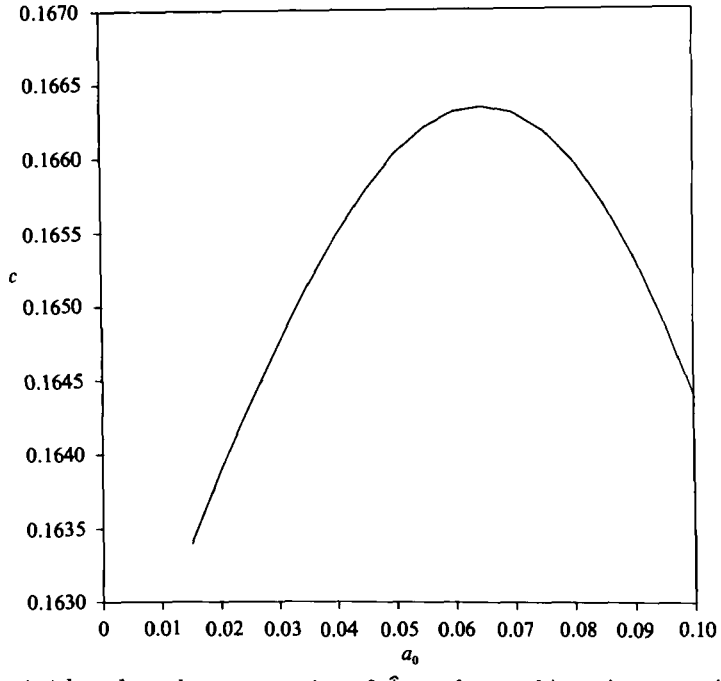

FIGURE 15. $c(a_0)$ based on the conservation of $\hat{A}$. $c \approx \frac{1}{6}$ over this entire range, implying that any unstable two-vortex configuration may evolve close to a 6:1 ellipse.

inviscid (or complete) transition is possible over a large range of a_0. $c(a_0)$, shown in figure 15, is everywhere close to $\frac{1}{6}$ – a 6:1 ellipse. This is an intriguing result since actual nonlinear evolution of two vortices does pass through a state nearly that of a 6:1 ellipse, and this transition occurs in a moderate time. Overman & Zabusky (1982) show the evolution of a perturbed unstable 2-vortex state in their figure 7, and, at a later time, a 6:1 ellipse is present. In quite a different context, in a simulation of a shear layer using a cloud of point vortices, Christiansen & Zabusky (1973) show the 2-vortex to 6:1 ellipse evolution in their figure 6. Since figure 14 allows such a wide range of transitions, it is not surprising that the 6:1 ellipse is observed so often in vortex-evolution problems. But Love (1893) showed that an ellipse is unstable if $c < \frac{1}{3}$, which makes a 6:1 ellipse unstable, thus this ellipse may evolve into another configuration – in fact, Dritschel (1985) shows with nonlinear calculations that the ellipse can break up into a 2-vortex state, but we defer the details to that study. Other inviscid transitions between an ellipse and the N-vortex states are possible. The complete list is given in table 2. Here a_1^*/a is the ratio of the scaling for the N-vortex state (see figure 1) to that of the ellipse. As N increases, the eccentricity of the ellipse increases. For severely stretched initial vorticity fields, stable final states are possible for 3, 4, 5 and 6 vortices. Note that a highly eccentric ellipse is essentially a finite-length vortex sheet.

As a final example, inviscid and nearly inviscid transitions were sought between an annular vortex and the corotating vortices. The annular vortex has a distribution given by

$$\omega(r) = \left\{ \begin{matrix} 0 & (r < a), \\ 1 & (a < r < b), \\ 0 & (r > b), \end{matrix} \right\} \tag{10.20}$$

N	a_0	c	a_1^*/a
2	0.039	0.1655	0.822
2	0.087	0.1654	0.818
3	0.62†	0.042	0.615
4	0.78†	0.020	0.560
5	0.86†	0.008	0.538
6	0.91†	0.005	0.525
7	0.95	0.003	0.514

TABLE 2. Inviscid transitions between N-states (N, a_0, a_1^*) and ellipse (c, a).
† Denotes a stable configuration.

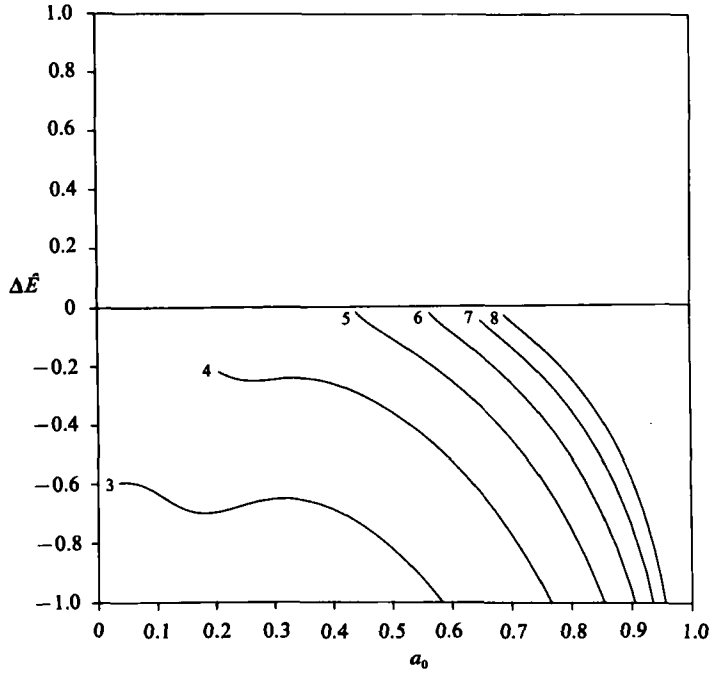

FIGURE 16. The transition dissipation $\Delta\hat{E}$ versus a_0 for the N-vortex to annular-vortex transition.

and the following analytical expressions for $\hat{E}$ and $\hat{A}$:

$$\left.\begin{aligned} \hat{E} &= 1-u-u^2\log c+2\log(1+c^2), \\ \hat{A} &= \frac{1-c^2}{1+c^2}, \end{aligned}\right\} \tag{10.21}$$

where

$$c=\frac{a}{b}, \quad u=\frac{2c}{1-c^2}. \tag{10.22}$$

As $c\to 1$, $\hat{E}\to 2\log 2$. $c(a_0)$ determined from $\hat{A}$-conservation *always* has $c > 0.6$, which, according to Snow (1978), implies that the annular vortex is always unstable in any transition to multiple vortices (the annular vortex is unstable for $c > \frac{1}{2}$). Figure 16 shows $\Delta\hat{E}$ for this transition, where $\hat{E}_i = \hat{E}(N\text{-state})$ and $\hat{E}_f = \hat{E}(\text{annulus})$. $\Delta\hat{E}$ is

always less than zero, and the transition with the least dissipation is between the largest (computed) member of the 5-vortex family and a $c \approx 0.7$ annular vortex. Also, 6, 7 and 8 vortices have small $\Delta\hat{E}$ (possible) transitions to an annular vortex. Since the solutions with the smallest value of a_0 have not yet been found for 4 or more vortices, we suspect that yet-smaller $\Delta\hat{E}$ annular vortex transitions may occur. Recall from §4 our suggestion that the families of N-vortex states pass continuously into wavy annular vortices for $N \geqslant 4$ in analogy with the results of Pierrehumbert & Widnall (1981) for the street of vortices. The energetic similarities between large-N-vortex states and certain annular vortices (albeit non-wavy) support our hypothesis.

The energy theory discussed in this section allowed us to restrict the evolution of unstable near-equilibrium vortex configurations. Viscous flow evolution turns out to be the least restricted – we may only say that the total energy must decrease as the initial vorticity distribution diffuses. 'Nearly' inviscid flow evolution allowed the possibility for transitions between near-equilibrium configurations provided that the timescale of the transition is much smaller than the viscous timescale. Viscous effects such as the smearing out of the initial distribution are small, of the order of this timescale ratio. An alternative and potentially more useful interpretation of nearly inviscid transitions associates the amount of dissipation with the incompleteness of an inviscid transition. Purely inviscid transitions rarely occur owing to the large number of constraints (due to the many conserved global quantities). Only the ellipse and the corotating vortices may possibly make inviscid transitions. Nonlinear calculations have proved that such transitions occur between two vortices and an ellipse. There are many more possible nearly inviscid transitions between ellipses and two vortices and between annular vortices and five or more corotating vortices.

11. Relation of stability properties to energetics

This section is meant to clarify the extent to which energy can determine stability. Since there seems to be some confusion about this point in the literature, a detailed derivation of the condition sufficient for stability will be presented.

Consider a system for which a conserved energy function $T(v_1, v_2, \ldots, v_n)$ exists. $v_1, \ldots, v_n$ are the state variables which completely describe the system. For example, in the context of constant-vorticity vortices, the vs can be thought of as coordinates of the discretized boundaries. Let

$$v_k = v_{0k} + \tilde{v}_k(t), \quad k = 1, 2, \ldots, n\ (\to\infty), \tag{11.1}$$

where v_{0k} corresponds to the stationary or steady state, t is the time and $\tilde{v}_k(t)$ is an admissible perturbation. Since we have a conservative system,

$$T(v_1, \ldots, v_n) = \text{constant} \equiv \bar{T}.$$

Meanwhile, $T(v_{01}, \ldots, v_{0n}) = \text{constant} \equiv T_0$. Expanding $\bar{T}$ in a Taylor series about the steady state, we find

$$\bar{T} = T_0 + \sum_i \frac{\partial T}{\partial v_i}\tilde{v}_i + \sum_i \sum_j \tilde{v}_i \frac{\partial^2 T}{\partial v_i \partial v_j}\tilde{v}_j + \ldots. \tag{11.2}$$

The steady states have the property that

$$\sum_i \tilde{v}_i \frac{\partial T}{\partial v_i}(v_{01}, \ldots, v_{0n}) = 0, \tag{11.3}$$

where the perturbation $\tilde{v}$ must conserve vortex area. In other words, the steady state is a stationary point of the energy functional with regard to area-preserving perturbations. Unfortunately, a translucent proof of this fact does not appear in the literature, but a relevant discussion can be found in Arnol'd (1965). Then the second term on the right-hand side of (11.2) is zero. The third term determines stability. If the matrix $\partial^2 T/\partial v_i \partial v_j$ is positive-definite or negative-definite (i.e. if all of its eigenvalues are of the same sign) then it is a *sufficient* condition for *stability*. Definiteness implies that, in a suitable transformed basis, the quadratic term in (11.2) is a sum of all positive or all negative terms, whose sum can equal $\overline{T}-T_0$ only when the perturbations are small and remain small for all time. On the other hand, if $\partial^2 T/\partial v_i \partial v_j$ is not definite, the stationary point is a saddle point of energy, and the perturbations could grow arbitrarily large while keeping $\overline{T}-T_0$ fixed at its initial small value. Of course, this does not prove that instability invariably occurs in this situation; it just shows that it is not ruled out.

The main practical difficulty in applying the energy argument is that one must know the properties of the second variation of energy *with respect to all admissible perturbations*. This information cannot be rigorously obtained from the knowledge of $\hat{E}(a_0)$ for the equilibrium states alone. Hence one must invariably resort to some indirect argument when attempting to determine whether a given state is a saddle point or an absolute minimum or maximum.

Saffman & Szeto (1980) applied a brief argument of this nature in an attempt to determine the value of a_0 at which the corotating two-vortex state becomes unstable. In terms of our notation, their argument can be paraphrased as follows. (Inconsequential differences in the form of the argument arise owing to notational differences.) First note that $\hat{E}$ has a minimum at $a_0 = 0.066$, where the area is a maximum. Thus, if we write $\hat{E}$ as a function of area $\hat{A}$, the energy curve consists of a high-energy branch and a low-energy branch, which meet at the point of maximum area (corresponding to $a_0 = 0.066$). This situation is represented by the (solid and dashed) lines in figure 17. It is implicitly assumed that *all* equilibrium states for a given area have been found, so that there are no other solution branches. Suppose that the higher-energy branch were a saddle or absolute minimum of energy. Then, since the energy is bounded above for fixed area and J, upon following the energy surface upward we would (it is presumed) eventually encounter an absolute maximum of energy.† This would be a contradiction, as the maximum would be a new steady state. Hence the higher-energy branch must be an absolute maximum, and therefore stable. Without making their reasoning explicit, Saffman & Szeto then hypothesize that the lower-energy branch is a saddle point, and thus presumably unstable; the point $a_0 = 0.066$ where the two branches join would then be the stability boundary.‡

Our calculations show, in contrast, that part of the higher-energy branch is unstable, with the instability setting in at $a_0 = 0.083$. This state of affairs is

† The mathematical underpinning of this argument is weak. It relies on the assumption that a functional defined on a given space and bounded above on that space attains a maximum *for some member of that space*. This assumption is true only if the functional is continuous and the space is compact. We note, however, that infinite-dimensional spaces of bounded norm are never compact. This is an elementary consequence of the theorem of F. Riesz (Dieudonné 1969).

‡ Owing to the sensitivity of the $\hat{E}$ and $\hat{A}$ calculations, it is difficult to calculate precisely the point a_0 where $\hat{E}$ and $\hat{A}$ reach extrema. For this reason, Saffman & Szeto (1980) actually predicted $a_0 = 0.077$ as their stability boundary; in their table 2 their J is related to $\hat{A}$ by $J = 1/\pi\hat{A}$ and reaches a minimum at $J = 0.8945$ or $\hat{A} = 0.3233$, corresponding to $a_0 = 0.077$. Since they claimed that the minimum in J determines the stability boundary, their correct value of a_0 would be 0.066, which we have verified to this number of digits.

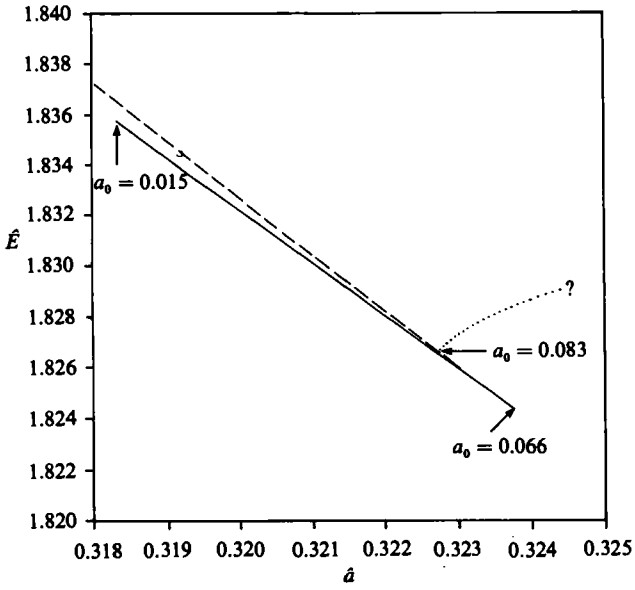

FIGURE 17. $\hat{E}(\hat{A})$ for two vortices. The dashed line represents stable symmetric solutions ($g(\theta) = g(-\theta)$). For $a_0 < 0.083$ these solutions become unstable (solid line). The dotted line represents the hypothetical stable asymmetric solutions.

inconsistent with the argument stated above. It is possible that the energy argument is essentially correct, but fails only because of an incomplete picture of the solution space. In particular, note that the instability sets in at $a_0 = 0.083$ via an exchange of stabilities, so that a zero eigenvalue appears at this point. This implies a bifurcation to a new solution branch at $a_0 = 0.083$; because the corresponding eigenmode is not symmetric about the line joining the vortex centres, the indicated bifurcation is to an asymmetric family of solutions. If this family has higher energy than the upper symmetric branch (as sketched in figure 17) then the upper symmetric branch could become a saddle past the bifurcation point without contradiction, since the energy surface could then be followed upward until the absolute energy maximum associated with the asymmetric branch was encountered. This idea could be tested by explicitly computing the asymmetric branch. Unfortunately, we have not yet succeeded in devising an algorithm to compute these asymmetric states.

Our numerically determined stability boundary proved to be insensitive to resolution. We doubled both the number of boundary points per vortex (to 288) and the number of Galerkin functions (to 41) independently and in combination, with no noticeable change in the stability-boundary position; however, the growth rates did increase by approximately 10%. With quadrupled resolution (576 boundary points and 81 Galerkin functions) the growth rates increased by only 1%, indicating convergence. As a separate confirmation of these results, we devised a numerical algorithm similar to that used by Overman & Zabusky (1982) and used it to calculate the evolution of perturbed vortices (for more details see Dritschel 1985). Starting with an $a_0 = 0.08$ unstable configuration with its unstable eigenmode superimposed (the initial perturbation amplitude being $\epsilon = 0.01$), we found linear and nonlinear instability after less than one period of rotation (Dritschel 1985). On the other side of the presumed stability boundary, at $a_0 = 0.085$, we added a supposedly neutral disturbance of amplitude $\epsilon = 0.0015$ (so that $a_0 - \epsilon > 0.083$) and ran the calculation

out to 10 rotation periods with no sign of instability. We ensured the accuracy of this calculation by verifying that the relative changes in J and Γ were less than 5×10^{-5}. So, we conclude that the initial-value calculations put the stability boundary in the range $0.08 < a_0 < 0.085$, in agreement with the matrix method. Finally, we note that Overman & Zabusky (1982) claimed to have found a displacement-like instability for two vortices when $a_0 = 0.10$, which is inconsistent with the results of the current study. The explanation is as follows. Their perturbation consisted of pushing both vortices inwards by a distance 0.005. This disturbance has the same area as the equilibrium state but *not* the same angular momentum J; in contrast, our calculations preserve *both* area and angular momentum, a requirement imposed by Thomson (1883) as well. Furthermore, since area and J are independent functions of a_0, a simple scale transformation cannot liken the J-changing perturbation to an area- and J-preserving perturbation of another (symmetric) two-vortex state.

Finally, we briefly review what happens for more than two vortices. Three and four vortices also go unstable through an exchange of stabilities, suggesting that there could be additional asymmetric solutions. Five and six vortices, on the other hand, become unstable only to oscillatory instabilities. With regards to the energy/area diagrams, three and four vortices also have values of a_0 where $\hat{E}$ and $\hat{A}$ have common extrema (5–8 vortices exhibit no energy or area extrema). Three vortices have two such points, while four vortices have just one point (see figures 12 and 13). In all cases the energy/area diagrams show cusps occurring at these special values of a_0. This is because both $\mathrm{d}^2\hat{E}/\mathrm{d}a_0^2$ and $\mathrm{d}^2\hat{A}/\mathrm{d}a_0^2$ are continuous through these points. However, as with two vortices, there is no correspondence between the matrix-determined stability boundary and the values of a_0 at which the extrema are obtained.

12. Conclusions

We began by calculating the equilibrium configurations of finite-area corotating vortices in an attempt to generalize Thomson's stability problem. In the process, we derived an expansion to fourth order in $(1-a_0)/(1+a_0)$ which both closely fits the exact results and explains the boundary distortion due to the number of vortices. Not only was this expansion used to confirm the numerically calculated boundary shapes, but, in fact, the numerical results verified the correctness of the expansion in all respects. We also found that we could very well approximate the true rotation period by a quantity based upon point-vortex ideas.

Having determined the equilibrium families of solutions, we set out to calculate their linear stability. First, we formally derived the stability equation and pointed out a symmetry property that significantly reduced the complexity of the problem. Finally, we solved this simplified problem numerically and determined the linear stability of corotating vortices. We verified that our results agree with Thomson's (1883) in the limit of small vortices and also found seven vortices, known to be neutrally stable if they are points, unstable for any finite area. Six or fewer vortices behaved quite differently, only becoming unstable for large size. Also, six or fewer vortices go unstable via boundary instabilities, which cannot happen for point vortices. Point vortices go unstable purely to displacement instabilities; seven or more vortices, even if finite-sized, also destabilize in this way.

A new expression for the energy of a two-dimensional fluid was formulated in order to extend the linear stability results. Specifically, energetics restricts the evolution of slightly perturbed equilibrium configurations; consequently, one can examine both nonlinear stability (Dritschel 1985) and the possibility of transitions between

near-equilibrium states. The latter issue was considered here by considering inviscid, 'nearly inviscid' and viscous evolution. Inviscid evolution is highly constrained owing to the large number of conserved quantities, and we only found a few examples in which inviscid evolution could possibly occur. In one example, nonlinear calculations (see Dritschel 1985) have confirmed that a certain member of the family of two vortices may make a transition to a nearly 6:1 ellipse – and vice versa. We also developed a theory for constraining two-dimensional flow based upon the smallness of the ratio of the dynamical timescale to the viscous timescale. We defined a 'nearly inviscid' transition as one for which this timescale ratio is very small. Such a transition would see little in the way of viscous effects such as the smoothing of the piecewise-constant vorticity distribution. However, a more fruitful interpretation of 'nearly inviscid' transitions translates the amount of dissipation during a transition into the incompleteness of a correspondingly inviscid transition or a measure of how close one can expect the initial state to come to a presumed final or subsequent state. Numerous transitions of this nature were found to be possible: between ellipses and corotating vortices and between annular vortices and five or more vortices.

The energy results of this study furthermore suggest that the families of four or more vortices pass continuously into a single wavy annular vortex in much the same way that the infinite row of vortices considered by Pierrehumbert & Widnall (1981) pass continuously into a wavy finite-thickness vortex sheet. Our hypothesis has yet to be confirmed, however.

Finally, in our efforts to resolve energy's relation to stability, we have found that much care has to be exercised. One cannot generally determine the unstable members of a family of equilibrium solutions merely by considering this family's energy and area (as defined in § 10). If other families of solutions are present, any argument based upon energy versus area must take into account these other families of solutions – we need (at least) a complete picture of the solution space.

The sequel to this study is presented in Dritschel (1985). There we numerically determine the nonlinear stability of N corotating vortices, the ellipse and the annular vortex. By tracking the long-time evolution, we capture transitions between various members of these families of equilibrium solutions, further confirming the energy theory. We find a close connection between energy and *non*linear stability and offer a few more words regarding linear stability.

This work has been submitted in partial fulfilment of the requirements for the degree of Ph.D. in the Geophysical Fluid Dynamics Program of Princeton University. The author is indebted to his thesis advisor, Dr R. T. Pierrehumbert, for much advice in matters of exposition and substance.

Appendix A: The matrix-eigenvalue problem

For any variable τ, let

$$\tau_0 \equiv \text{unperturbed basic state},$$

$$\tau' \equiv \text{perturbation},$$

$$\tau = \tau_0 + \tau' \equiv \text{entire quantity},$$

$$\hat{\tau} \equiv \text{time-independent part of } \tau' = \hat{\tau}\, e^{\sigma t},$$

where σ is a generally complex growth rate to be determined as an eigenvalue. The entire velocity in the rotating frame on the jth vortex is

$$\boldsymbol{u}_j \equiv \boldsymbol{u}(\boldsymbol{x}_j) = -\frac{1}{4\pi}\sum_{k=1}^{N}\int_0^{2\pi} \log r_{jk}^2 \frac{\mathrm{d}\boldsymbol{X}_k}{\mathrm{d}\theta}\,\mathrm{d}\theta + \boldsymbol{\Omega}(y_j, -x_j), \tag{A 1}$$

where

$$\left.\begin{aligned} \boldsymbol{x}_j &= (x_j, y_j) = (r_0 c_j + g_j(\alpha, t)\cos(\alpha+\theta_j),\ r_0 s_j + g_j(\alpha, t)\sin(\alpha+\theta_j)),\\ \boldsymbol{X}_k &= (X_y, Y_j) = (r_0 c_k + g_k(\theta, t)\cos(\theta+\theta_k),\ r_0 s_k + g_k(\theta, t)\sin(\theta+\theta_k)),\\ r_{jk}^2 &= |\boldsymbol{x}_j - \boldsymbol{X}_k|^2. \end{aligned}\right\} \tag{A 2}$$

With some algebraic ingenuity, we find (using a slightly different notation than that in §5)

$$\begin{aligned} \hat{u}_j = {} & \frac{1}{2\pi}\sum_{k=1}^{N}\int_0^{2\pi} \hat{g}_k(\theta)\frac{(\mathrm{d}X_{0k}/\mathrm{d}\theta)\sin(\theta+\theta_k) - (\mathrm{d}Y_{0k}/\mathrm{d}\theta)\cos(\theta+\theta_k)}{r_{0jk}^2}(y_{0jk}, -x_{0jk})\,\mathrm{d}\theta \\ & - \frac{\hat{g}_j(\alpha)}{2\pi}\sum_{k=1}^{N}\int_0^{2\pi}\frac{(\mathrm{d}X_{0k}/\mathrm{d}\theta)\sin(\alpha+\theta_j) - (\mathrm{d}Y_{0k}/\mathrm{d}\theta)\cos(\alpha+\theta_j)}{r_{0jk}^2}(y_{0jk}, -x_{0jk})\,\mathrm{d}\theta \\ & + \Omega\hat{g}_j(\alpha)(\sin(\alpha+\theta_j), -\cos(\alpha+\theta_j)). \end{aligned} \tag{A 3}$$

Equation (5.8) can be rewritten as

$$\sigma\hat{g}_j = -u_{0\theta}\frac{\mathrm{d}}{\mathrm{d}\alpha}\left[\frac{\hat{g}_j}{g_0}\right] + \frac{1}{u_{0\theta}}(\hat{u}_j v_{0j} - \hat{v}_j u_{0j}), \tag{A 4}$$

where

$$\frac{1}{g_0}\frac{\mathrm{d}g_0}{\mathrm{d}\alpha} = \frac{u_{0r}}{u_{0\theta}} \tag{A 5}$$

(the statement that the unperturbed boundary has no flow across it) has been used. u_{0r} and $u_{0\theta}$ do not depend on the vortex j – only upon α. From (5.3) we take $\hat{g}_j(\alpha)$ as

$$\hat{g}_j(\alpha) = g_0(\alpha)\gamma_j(\alpha), \quad \text{where} \quad \gamma_j(\alpha) = \sum_{m=1}^{M} C_m{}^j \phi_m(\alpha). \tag{A 6}$$

Also, we introduce the following notational abbreviations:

$$\left.\begin{aligned} \langle(\,)\rangle &= \frac{1}{2\pi}\int_0^{2\pi}(\,)\,\mathrm{d}\theta, \quad \Sigma = \sum_{k=1}^{N}, \quad b_{jk}{}^x(\theta;\alpha) = \frac{x_{0jk}}{r_{0jk}^2}, \quad b_{jk}{}^y(\theta;\alpha) = \frac{y_{0jk}}{r_{0jk}^2},\\ Q_k(\theta) &= \frac{\mathrm{d}X_{0k}}{\mathrm{d}\theta}\cos(\theta+\theta_k) - \frac{\mathrm{d}Y_{0k}}{\mathrm{d}\theta}\sin(\theta+\theta_k) = -g_0,\\ Q_{jk}(\theta;\alpha) &= \frac{\mathrm{d}X_{0k}}{\mathrm{d}\theta}\cos(\alpha+\theta_j) - \frac{\mathrm{d}Y_{0k}}{\mathrm{d}\theta}\sin(\alpha+\theta_j). \end{aligned}\right\} \tag{A 7}$$

Equation (A 3) can then be rewritten as

$$\left.\begin{aligned} \hat{u}_j &= \Sigma\langle\hat{g}_k(\theta)\,Q_k\,b_{jk}{}^y\rangle + \hat{g}_j(\alpha)(\Omega\sin(\alpha+\theta_j) - \Sigma\langle Q_{jk}\,b_{jk}{}^y\rangle),\\ \hat{v}_j &= -\Sigma\langle\hat{g}_k(\theta)\,Q_k\,b_{jk}{}^x\rangle - \hat{g}_j(\alpha)(\Omega\cos(\alpha+\theta_j) - \Sigma\langle Q_{jk}\,b_{jk}{}^x\rangle). \end{aligned}\right\} \tag{A 8}$$

Equation (A 4) is now rewritten in terms of the γ_j, and we define

$$\epsilon_j = \sigma\gamma_j + \frac{u_{0\theta}}{g_0}\frac{\mathrm{d}\gamma_j}{\mathrm{d}\alpha} - \frac{1}{g_0 u_{0\theta}}(\hat{u}_j v_{0j} - \hat{v}_j u_{0j}) \neq 0. \tag{A 9}$$

$\epsilon_j \neq 0$ unless $M = \infty$, whereupon the disturbances are fully representable in terms of the orthonormal set of basis functions $\{\phi_m\}$. For practical reasons, all the ϕ_m, $m = 1, 2, \ldots$, cannot be kept. The Galerkin approach to keeping only a finite number M of terms is to make the error ϵ_j orthogonal to each of the basis functions:

$$\int_0^{2\pi} \epsilon_j \phi_n \,\mathrm{d}\alpha = 0, \quad n = 1, \ldots, M, \quad j = 1, \ldots, N. \tag{A 10}$$

This requirement yields MN equations for the same number of unknowns: $C_n{}^j$, $n = 1, \ldots, M$, $j = 1, \ldots, N$. This yields (5.12) after introducing the following definitions:

$$\left.\begin{aligned}
B_j(\alpha) &= \frac{u_{0j}}{u_{0\theta}}(\Omega\cos(\alpha+\theta_j) - \Sigma\langle Q_{jk} b_{jk}{}^x\rangle) + \frac{v_{0j}}{u_{0\theta}}(\Omega\sin(\alpha+\theta_j) - \Sigma\langle Q_{jk} b_{jk}{}^y\rangle),\\
D_m{}^{jk}(\alpha) &= \frac{u_{0j}}{g_0 u_{0\theta}}\langle\phi_m g_0 Q_k b_{jk}{}^x\rangle + \frac{v_{0j}}{g_0 u_{0\theta}}\langle\phi_m g_0 Q_k b_{jk}{}^y\rangle,\\
E_{mn}{}^j &= \int_0^{2\pi}\mathrm{d}\alpha\left(B_j\phi_m - \frac{u_{0\theta}}{g_0}\frac{\mathrm{d}\phi_m}{\mathrm{d}\alpha}\right)\phi_n,\\
F_{mn}{}^{jk} &= \int_0^{2\pi}\mathrm{d}\alpha\, D_m{}^{jk}\phi_n,\\
A_{mn}{}^{jk} &= \delta_{jk} E_{mn}{}^j + F_{mn}{}^{jk}.
\end{aligned}\right\} \tag{A 11}$$

The result restated here is

$$\sigma C_n{}^j = \sum_{k=1}^{N}\sum_{m=1}^{M} A_{mn}{}^{jk} C_m{}^k, \quad j = 1, \ldots, N, \quad n = 1, \ldots, M. \tag{A 12}$$

Appendix B. Point-vortex stability and the stability of eight vortices

This appendix presents a drastically simplified derivation and explanation of the stability of any number of point vortices. This simplification came as a result of the symmetry properties outlined in §6. It also clears up some further errors made by Thomson. It was pointed out during the preparation of this manuscript that the result below was first derived by Havelock (1931).

Equations taken from and sections refered to in Thomson (1883) will be surrounded in curly brackets. Then equations {107} and {111} using the second equation in section {51} are (in non-dimensional form)

$$\frac{\mathrm{d}x_s}{\mathrm{d}t} = \frac{N^2-1}{6}\theta_s - \sum_{k=1}^{N}\frac{\theta_k}{1-c_{ks}} \quad (k \neq s), \tag{B 1}$$

$$\frac{\mathrm{d}\theta_s}{\mathrm{d}t} = \frac{(N-1)(N-11)}{6}x_s - \sum_{k=1}^{N}\frac{x_k}{1-c_{ks}} \quad (k \neq s), \tag{B 2}$$

where x_s is the perturbation radial displacement and θ_s is the perturbation angular displacement of the sth vortex, while $c_{ks} = \cos(2\pi(k-s)/N)$. The first terms on the

right-hand sides of these equations come from sums to be evaluated later (Thomson claimed to have evaluated them by trigonometry). Thomson further requires

$$\sum_{s=1}^{N} x_s = 0, \quad \sum_{s=1}^{N} \theta_s = 0 \tag{B 3}$$

(see the end of section {48}). The first expresses the conservation of angular momentum, while the second simply ignores the neutral mode, which rigidly rotates the entire configuration.

The symmetry arguments of §6 (especially (6.10)) along with (B 3) suggest

$$x_s = \alpha\omega^{ps}, \quad \theta_s = \beta\omega^{ps}, \quad p = 1, 2, \ldots, N-1, \tag{B 4}$$

where $\omega = \cos(2\pi/N) + \mathrm{i}\sin(2\pi/N)$ and the real part is intended. p cannot be a multiple of N, because this would violate (B 3). p indicates the symmetry of the mode, and is analogous to the l introduced in §6 ($p = l-1$). Substituting this into (B 1) and (B 2) yields

$$\frac{\mathrm{d}\alpha}{\mathrm{d}t} = \beta(\tfrac{1}{6}(N^2-1) - S_p), \quad \frac{\mathrm{d}\beta}{\mathrm{d}t} = \alpha(\tfrac{1}{6}(N-1)(N-11) - S_p), \tag{B 5}$$

where

$$S_p = \sum_{\substack{k=1 \\ k\neq s}}^{N} \frac{\omega^{p(k-s)}}{1-c_{ks}} = \sum_{\substack{k=1 \\ k\neq s}}^{N} \frac{\cos(2\pi p(k-s)/N)}{1-\cos(2\pi(k-s)/N)} = \sum_{k=1}^{N-1} \frac{\cos(2\pi pk/N)}{1-\cos(2\pi k/N)}, \tag{B 6}$$

because the sine series is exactly zero and $k-s$ can be regarded as a dummy variable. Hence (B 5) is independent of s, as required. So,

$$\frac{\mathrm{d}^2\alpha}{\mathrm{d}t^2} = \sigma_p^2\alpha, \quad \sigma_p^2 = (\tfrac{1}{6}(N^2-1) - S_p)(\tfrac{1}{6}(N-1)(N-11) - S_p). \tag{B 7}$$

Moreover, a simple analytical expression for S_p has been found:

$$S_p = \tfrac{1}{6}(N-1)(N-5) + (p-1)(p+1-N). \tag{B 8}$$

Specifically, $S_0 = \frac{1}{6}(N^2-1)$, $S_1 = \frac{1}{6}(N-1)(N-5)$ and $S_1 - (N-1) = \frac{1}{6}(N-1)(N-11)$, which accounts for the terms in (B 1) and (B 2). This sum has the property $S_p = S_{N-p}$, so that $\sigma_p = \sigma_{N-p}$, and there are at most $[\frac{1}{2}N]$ distinct eigenvalues corresponding to the symmetries $p = 1, 2, \ldots, [\frac{1}{2}N]$ (here [ ] means 'integer value of'). The final expression for σ_p^2 is

$$\sigma_p^2 = (p-1)^2(p+1-N)^2 - (N-1)^2, \tag{B 9}$$

valid for all N. Dimensionally, this must be multiplied by $m^2/4\pi^2r^4$ in Thomson's notation ($m \equiv$ the strength of one vortex, $r \equiv$ the radius of the circle they all lie upon in equilibrium).

Thomson makes a few mistakes in his treatise with regards to certain eigenvalues which violate the constraints in (B 3). The eigenvectors indicate that these disturbances are symmetric and are therefore not allowed. The largest negative eigenvalues listed for five or more vortices by Thomson are disallowed by the constraints.

The neutral mode for $N = 7$ vortices comes from $p = 3$ and 4 ($l = 4$ and 5), and the numerical results agree with this. Eight vortices have two unstable modes: $\sigma_4^2 = 32$ (every other vortex is displaced the same way) and $\sigma_3^2 = 15$ (complicated eigenvector). In the numerical calculation, the two growth rates are $r_4 = 5.077569$ and $r_3 = 3.476346$ for $a_0 = 0.995$. The conversion from r to σ is

$$\sigma_p = \frac{N-1}{2\pi} r_p. \tag{B 10}$$

The numerically computed σ_p^2 are 31.99986 and 14.99969 respectively.

To achieve these excellent results, the boundary shapes for small vortices had to be calculated very accurately. The approximate results of §3 were used as the first guess in the iterative procedure to find the precise boundary shapes; the error in the computed shapes was less than 5×10^{-7}.

Finally, the numerical code had to be very careful to accurately calculate the integrals involving the singular terms $b_{jk}{}^{x}$ and $b_{jk}{}^{y}$ in (A 11). These integrals are functions of the angle α, and the integral is over θ. α must be evaluated on the regular, coarse grid (which has approximately equal angle spacing) and θ must be evaluated at the four Gaussian points between each coarse grid point. The singularity is of the form $1/(\alpha-\theta)$, and so does not contribute if evaluated in this way. The coarse α-points are then interpolated onto the Gaussian grid, whereupon the calculation continues. The 7- and 8-vortex calculations serve as a good check of this method.

REFERENCES

Arnol'd, V. 1965 Conditions for the nonlinear stability of stationary plane curvilinear flows of an ideal fluid. *Dokl. Akad. Nauk SSSR* **162**, 975–978. [English transl. *Sov. Maths* **6**, 331–334.]

Christiansen, J. P. & Zabusky, N. J. 1973 Instability, coalescence and fission of finite-area vortex structures. *J. Fluid Mech.* **61**, 219–243.

Dieudonné, J. 1969 *Foundations of Modern Analysis*, pp. 112–113. Academic.

Dritschel, D. G. 1985 The nonlinear stability of corotating uniform vortices. Submitted to *J. Fluid Mech.*

Havelock, T. H. 1931 The stability of motion of rectilinear vortices in ring formation. *Phil. Mag.* **11**, 617.

Lamb, H. H. 1932 *Hydrodynamics*. Dover.

Love, A. E. H. 1893 *Proc. Lond. Math. Soc.* **35**, 18.

Morikawa, G. K. & Swenson, E. V. 1971 Interacting motion of rectilinear geostrophic vortices. *Phys. Fluids* **14**, 1058–1073.

Overman, E. A. & Zabusky, N. J. 1982 Evolution and merger of isolated vortex structures. *Phys. Fluids* **25**, 1297–1305.

Pierrehumbert, R. T. 1980 A family of steady, translating vortex pairs with distributed vorticity. *J. Fluid Mech.* **99**, 129–144.

Pierrehumbert, R. T. & Widnall, S. E. 1981 The structure of organized vortices in a free shear layer. *J. Fluid Mech.* **102**, 301–313.

Poincaré, H. 1893 *Théorie des Tourbillons* (ed. G. Carré), chap. 4. Deslis Frères.

Saffman, P. G. & Schatzman, J. C. 1982 Stability of a vortex street of finite vortices. *J. Fluid Mech.* **117**, 171–185.

Saffman, P. G. & Szeto, R. 1980 Equilibrium shapes of a pair of uniform vortices. *Phys. Fluids* **23**, 2339–2342.

Snow, J. T. 1978 On inertial instability as related to the multiple-vortex phenomenon. *J. Atmos. Sci.* **35**, 1660–1667.

Thomson, J. J. 1883 *A Treatise on the Motion of Vortex Rings*, pp. 94–108. Macmillan.

Ting, L. 1983 On the application of the integral invariants and decay laws of vorticity distributions. *J. Fluid Mech.* **17**, 497–506.

Wu, H. M., Overman, E. A. & Zabusky, N. J. 1982 Steady-state solutions of the Euler equations in two dimensions: rotating and translating V-states with limiting cases. I. Numerical algorithms and results. *Univ. Pittsburgh Tech. Rep.* ICMA-82-44.